Bulletin of Volcanology (2020) 82:58
https://doi.org/10.1007/s00445-020-01397-1

RESEARCH ARTICLE

Late Cenozoic columnar-jointed basaltic lavas in eastern and southeastern China: morphologies, structures, and formation mechanisms

Yongquan Li[1,2] · Jianzhong Liu[3]

Received: 8 October 2018 / Accepted: 15 June 2020

Abstract
Late Cenozoic basaltic lavas in eastern and southeastern China commonly display spectacular columnar joints. In four volcanic fields in this region, we have observed and classified five types of colonnade (vertical, inclined, horizontal, fanning upwards, and fanning downwards) that provide information on the cooling regime and emplacement mechanism of the lava flows. In total, we analyzed the geometry and morphology of joints across ten different lava flow areas in the Changle volcanic field (CVF), Luhe volcanic field (LVF), eastern Zhejiang volcanic field (EZVF), and Niutoushan-Linjin Island-Nanding Island volcanic field (NLNVF). Field observations show that columnar-jointed alkaline basalts commonly exhibit narrow and irregular shapes indicating fast cooling. Tholeiites with columnar joints, in contrast, show wide and regular polygons, indicating slower cooling. Vertical columnar joints and other types (horizontal and fanning shaped) have different mature patterns, with the implication that lavas flowed on relatively flat land and in paleo-valleys, respectively. This study suggests a simple qualitative description of different types of colonnade can be made based on their alignment patterns, which represents a direct and easy way to derive solidification processes after lava eruption from colonnaded lavas in outcrop.

Keywords Columnar jointing · Lava flow unit · Lava cooling · Entablature · Colonnade

Introduction

Columnar jointing has been observed in lava flows, shallow sills, and dikes of all compositions around the world (Tomkeieff 1940; Spry 1962; Xu 1982; DeGraff and Aydin 1987; Lyle 2000; Hetényi et al. 2012; Phillips et al. 2013; Sheth et al. 2015; Moore 2019; Weinberger and Burg 2019) and on other planets (Milazzo et al. 2009). Most frequently, these cooling joints are observed in basalts, including the famous examples of Giant's Causeway (Bulkeley 1693) and Staffa (Phillips et al. 2013). Previous field (Tomkeieff 1940; Beard 1959; Peck and Minakami 1968; Long and Wood 1986; Goehring and Morris 2008; Bosshard et al. 2012; Hetényi et al. 2012; Phillips et al. 2013; Tanner 2013; Sheth et al. 2011, 2017a, b; Sheth 2018), experimental (e.g., Müller 1998a, b, 2001; Goehring et al. 2006), and theoretical (e.g., Mallett 1875; James 1920; Spry 1962; Ryan and Sammis 1978; Budkewitsch and Robin 1994; Grossbacher and McDuffie 1995; Goehring et al. 2009; Woodell 2009; Guy 2010; Lamur et al. 2018; Piombo and Dragoni 2018) works on the formation of these features have identified flow emplacement and environmental controls on the characteristics of columns. We here apply the theory described in this extensive body of literature on basaltic colonnades to investigate the emplacement conditions of Late Cenozoic columnar-jointed lavas in eastern and SE China.

Editorial responsibility: H. Dietterich

Electronic supplementary material The online version of this article (https://doi.org/10.1007/s00445-020-01397-1) contains supplementary material, which is available to authorized users.

✉ Yongquan Li
lyq@cugb.edu.cn

[1] School of Earth Sciences and Resources, China University of Geosciences, Beijing 100083, China

[2] Department of Geology, University at Buffalo, Buffalo, NY 14260, USA

[3] Institute of Geochemistry, Chinese Academy of Sciences, Guiyang 550002, China

Published online: 01 July 2020

In thick, columnar-jointed lava flows, a distinct tier of well-formed, regularly spaced, equal-sized, parallel columns is known as the colonnade (Fig. 1a, b; see also Tomkeieff 1940; Spry 1962). This tier is usually located in the lower parts of the lava flows and is overlain by a much thicker tier of irregularly shaped and haphazardly oriented columns, called the entablature (Fig. 1a, b; see also Long and Wood 1986; Lyle 2000). Meanwhile, small-scale structures, such as chisel marks or striae, are planar features on joint side surfaces (Fig. 1c) and are thought to be an expression of the incremental growth of colonnade joints (James 1920; Tomkeieff 1940; Spry 1962; Degraff and Aydin 1987; Goehring and Morris 2008; Tanner 2013). Classifications of colonnades into specific types, based on criteria such as column diameter and side

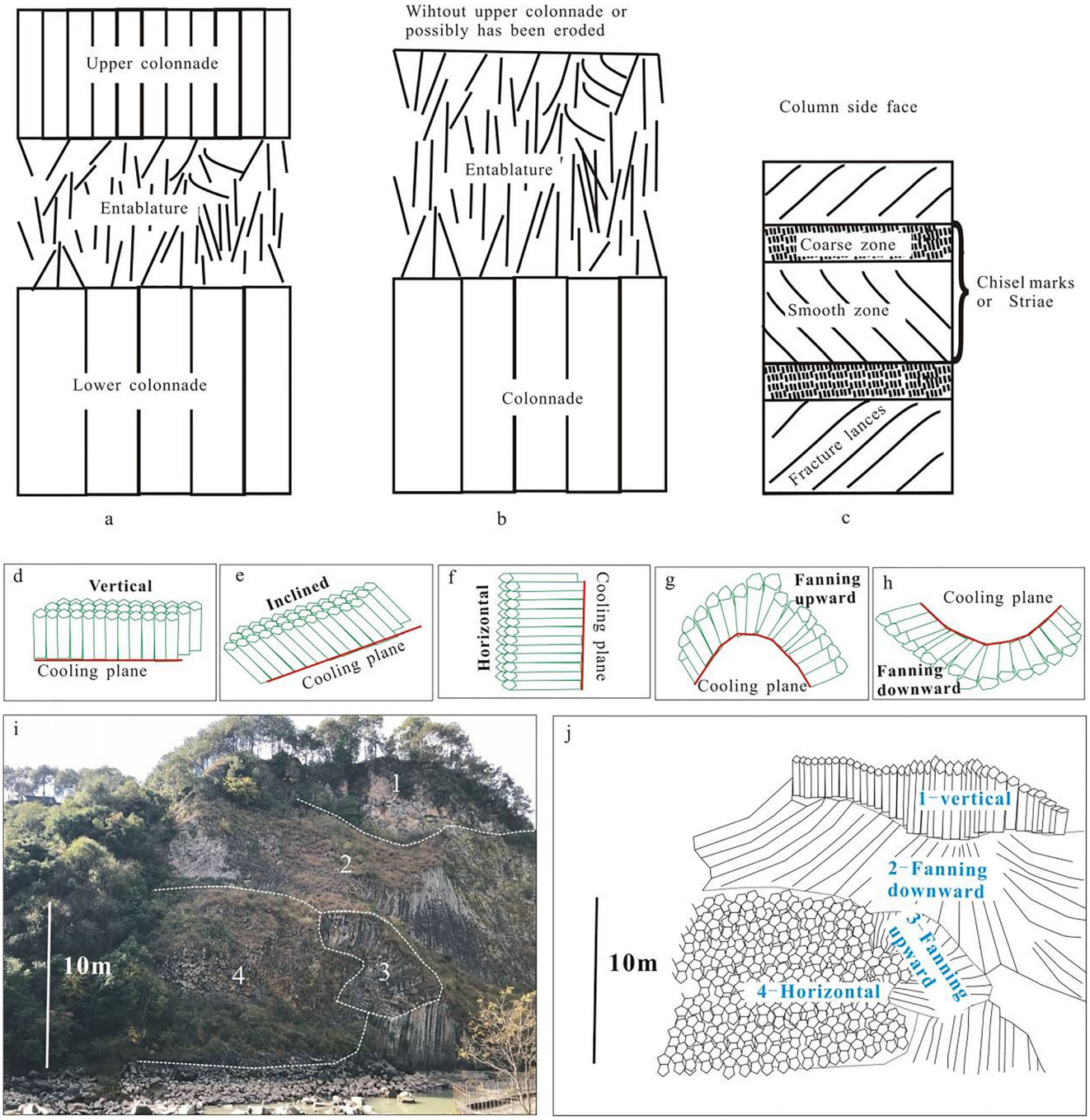

Fig. 1 **a**, **b** Schematic architecture of columnar-jointed lavas (after Lyle (2000) and Phillips et al. (2013)). **c** Interior structures on the side face of a column (after Xu (1984) and DeGraff and Aydin (1987)). **d**–**h** Schematic figures of the five colonnade patterns found in the volcanic fields of eastern and SE China. **i** An example of different types of colonnade patterns in a vertical section; the picture is from the Tengchong volcanic field (25° 13′ 21″ N, 98° 34′ 40″ E), Yunnan Province, SW China. **j** Schematic figure giving the interpretation of colonnade patterns of figure **i**

length (Xu 1982), the arrangement of colonnade and entablature in a single lava flow (Long and Wood 1986), and geometric patterns in the colonnade (Hetényi et al. 2012), are summarized in Table 1. These classifications are important for discriminating different types of colonnade by statistical treatment of field measurements (Goehring and Morris 2008; Phillips et al. 2013). We here use data and observations from the columnar-jointed lavas in eastern and SE China to assess and evolve such classification systems (Fig. 1d–j).

Spectacular colonnades outcrop in basaltic lava fields in eastern and SE China. Many researchers have studied the petrological and geochemical characteristics of these basaltic lava fields and discussed their emplacement mechanisms (Zou et al. 2000; Ho et al. 2003; Zhao et al. 2004; Zeng et al. 2010; Xu et al. 2012; Sakuyama et al. 2013; Li et al. 2015, 2016). However, there is a lack of studies with detailed field description that discriminate various units using morphological features and interior structures. The main motivation of this study is thus to describe and interpret the morphology of these columnar-jointed basaltic lavas, complementing our observations with statistical analysis of the colonnades (length, column diameter, shape and maturity, and striae height) and morphology of the interior (presence/absence of entablature). We discuss the possible eruptive environments of these columnar-jointed basaltic lavas and the formation mechanisms of their columnar jointing, providing a classification system linked to cooling environment. Our results from these Chinese basaltic volcanic fields complement existing studies of columnar jointing from elsewhere in the world.

Geological setting

Late Cenozoic basaltic lavas are generally located in East China and are mainly distributed in four regions (Fig. 2): (i) NE China (around the Songliao basin), (ii) eastern China (controlled by the Tanlu fault), (iii) SE China (controlled by a series of NE-SW or NNE-SSW strike-slip faults), and (iv) southern China (mainly located at the Leizhou Peninsula, northern Hainan Province, and adjacent areas). These basaltic lava flow fields are dominantly distributed along the continental margin (Fig. 2), which are generally controlled by regional abyssal faults (Niu et al. 2000; Ho et al. 2003). Eastern and SE China (Shandong, Jiangsu, Zhejiang, Fujiang, and Taiwan) are located along the easternmost margin of the Eurasian Plate where abundant outcrops of Cenozoic basaltic lavas occur. Early studies (Chung et al. 1995, 1997; Smith 1998; Zhao et al. 2004) indicated that all volcanism in eastern and SE China was likely attributed to mantle upwelling due to passive extension. However, more recent work has suggested that the formation of these Late Cenozoic basaltic lavas was most probably triggered by melting of dehydrated oceanic crust from the stagnant slab in the mantle transition zone (MTZ) which was associated with westward subduction of the Pacific Plate (Xu et al. 2012; Sakuyama et al. 2013; Li et al. 2015, 2016). Unlike NE China where Cenozoic basaltic lavas are quite widespread, Cenozoic basaltic lava flow fields in eastern and SE China are small and usually of monogenetic type (Fig. 2). However, these small volcanic fields (Changle, Guabushan, Guizishan, Niutoushan, and Nanding Islands) have been the focus of many studies by Chinese geologists

Table 1 Classifications of the colonnade patterns

No.	Classified method	Pattern	Evaluation	Reference
1	Based on the side length (L) and diameter (D) of hexagonal column	Large: $L > 1$ m and $D > 2$ m Medium: $L = \sim 1$–0.25 m and $D = 2$–0.5 m Small: $L < 0.25$ m and $D < 0.5$ m	This classification is very specific but needs large quantity of statistics	Xu (1982)
2	Geometric shape on transversal surface	Regular: primarily are hexagon Subregular: mostly are pentagon Irregular: mixture of 4-, 5-, 6-, 7-, and 8-side polygons	Conceptual classification not refers to their forming mechanism	Xu (1982)
3	Vertical section structure of colonnade	Type I: highly regular colonnade and lack an entablature Type II: repeated entablature and colonnade Type III: a lower colonnade and a single well-defined entablature in vertical section	This classification refers to their forming mechanisms and needs comprehensive observation	Long and Wood (1986)
4	Interior structure of colonnade	Single-unit flow (SUF): only single colonnade; multiple-unit flow (MUF) consists of 2 or more patterns of colonnade	This classification is very simple but not refers to their forming mechanisms	Hetényi et al. (2012)
5	Colonnade alignment pattern	Vertical: intersect angle of column and horizontal plane $\theta > 80°$ Inclined: $10° < \theta < 80°$ Horizontal: $\theta < 10°$ Fanning upward: upward scatter Fanning downward: downward scatter	This classification is very simple and can be made based on field observation but not refers to their forming mechanisms	A suggestion of this study

(Zhou and Chen 1981; Zhi 1990; Zhang and Lu 1997; Zou et al. 2000; Ho et al. 2003; Zhao et al. 2004; Zeng et al. 2010; Li et al. 2015, 2016) and commonly show spectacular columnar jointing structures.

Columnar-jointed basalts in eastern China are generally found in the Changle volcanic field in Shandong Province and in the Luhe volcanic field in Jiangsu Province (Fig. 2). This activity is linked to the Tanlu fault, a NE-SW strike-slip fault which controls the major tectonic units of eastern China (Niu et al. 2000). The Changle volcanic field (CVF, Fig. 2), ~ 19–12 Ma in age (Chen and Peng 1985; Du et al. 2009), is located west of the central part of the Tanlu fault. It consists of about 80 effusive vents, and its lavas cover an area of ~ 400 km^2 (Du et al. 2009; Chen et al. 2016). Lavas in the CVF and adjacent areas are primarily composed of strongly alkaline basalts, with lower contents of SiO_2 (< 45 wt%) and higher concentrations of incompatible elements, indicating that carbonate-bearing peridotite is likely the main source for the formation of these basaltic lavas (Table 4; Zeng et al. 2010; Sakuyama et al. 2013). The Luhe volcanic field (LVF, Fig. 2) is located east of the Tanlu fault. The main basaltic lavas of the LVF erupted at ~ 11–9 Ma (Chen and Peng 1988) and have an outcrop area of ~ 726 km^2 (Chen et al. 2014). Basaltic lavas in the LVF consist mainly of tholeiites and alkaline basalts (Table 4), which were probably derived from a mantle source by partial melting of pyroxenite/eclogite and peridotite (Li et al. 2016).

Columnar-jointed basalts in the Fujian and Zhejiang provinces are usually distributed along the coastal areas and include from SW to NE the Longhai, Minqing, Minxi, Quzhou, Linhai, and Shengzhou lavas (Ho et al. 2003). The eastern Zhejiang volcanic field (EZVF, Fig. 2) is a Neogene (~ 10.5–2.5 Ma) volcanic field covering ~ 700 km^2 area (Ho et al. 2003; Chen et al. 2014) and exhibits spectacular examples of columnar joints. These lavas are mainly composed of tholeiites (Table 4) and were probably generated by partial melting and mixing of magmas from the asthenospheric mantle (DM or MORB) and enriched lithospheric mantle (Ho et al. 2003). The Niutoushan-Linjin Island-Nanding Island volcanic field (NLNVF) formed at ~ 17.1–11.7 Ma (Ho et al. 2003) and is distributed along a NE-SW to NNE-SSW-trending belt. Two groups of basalts (low Ti and high Ti) have been identified in the Niutoushan lavas (Table 4), and the interaction between two types of magma (tholeiitic magma and alkaline magma) in the mantle is proposed for the formation of Niutoushan basalts (Zeng et al. 2017). Volcanic rocks outcropping in SE China may be controlled by a series of generally NE-SW-trending linear fissure systems located in SE China (Fig. 2). The preexisting regional structure (Ho et al. 2003) is likely the key factor in controlling the distribution of these basaltic lavas.

Fig. 2 Simplified tectonic units and distribution of the main Late Cenozoic basalts in China (modified from Chen et al. 2017). The locations of the lavas discussed here are marked by the *purple triangle*. CVF, Changle volcanic field; EZVF, eastern Zhejiang volcanic field; LVF, Luhe volcanic field; NLNVF, Niutoushan-Linjin Island-Nanding Island volcanic field

Methodology

The four volcanic fields investigated are located in relatively warm and humid areas (latitude < 40° N), which are covered by extensive sediments and vegetation. Therefore, we selected as our study sites sections in quarries where fresh outcrops occur. Their locations are listed in Table 2. The main aim of this study was to observe and systematically describe the morphologies and interior structures of the four basaltic lava fields. To achieve this, at each outcrop, we measured the thickness of each lava flow unit recorded as the number of constituent units and described their surface textures, as well as disposition of cooling joints and their patterns. We also characterized internal structures, including crystallinity and vesicularity; xenoliths; and striae or chisel marks within each unit.

Following Nichols (1936) and Walker (1972), a lava flow unit can be defined as having "a top which cooled significantly and solidified before another flow-unit was superimposed on it" so that "each flow-unit is a separate cooling unit" (Harris and Rowland 2009). Such effusive units (EUs) were defined and distinguished on the basis of a facies analysis following Cas and Wright (1987) and by tracing all the contacts required to delimit each unit.

Characterization of the columnar jointing included the measurement of column side length (L), counting the number of column sides (N), and defining the column density (number of polygons/m^2) (D) (Table 3). These measurements were conducted in the field using a tape measure with an accuracy of ± 1 cm. We used digital photographs of each column to refine our descriptions. We also collated all chemical compositions of data available for each volcanic field and added analyses of eight new samples (Table 4). Finally, a hexagonality index (Xn) was applied to assess the following pattern order (Budkewitsch and Robin 1994; Phillips et al. 2013):

$$Xn = \sqrt{(f5 + f7) + 4(f4 + f8) + 9(f3 + f9) + 16f10 + \ldots} \quad (1)$$

where fn is the fraction of column top faces with N sides, $Xn = 0$ represents all columns are in a six-sided pattern with a perfect order, while $Xn = 1$ indicates all columns are in five-sided and/or seven-sided pattern.

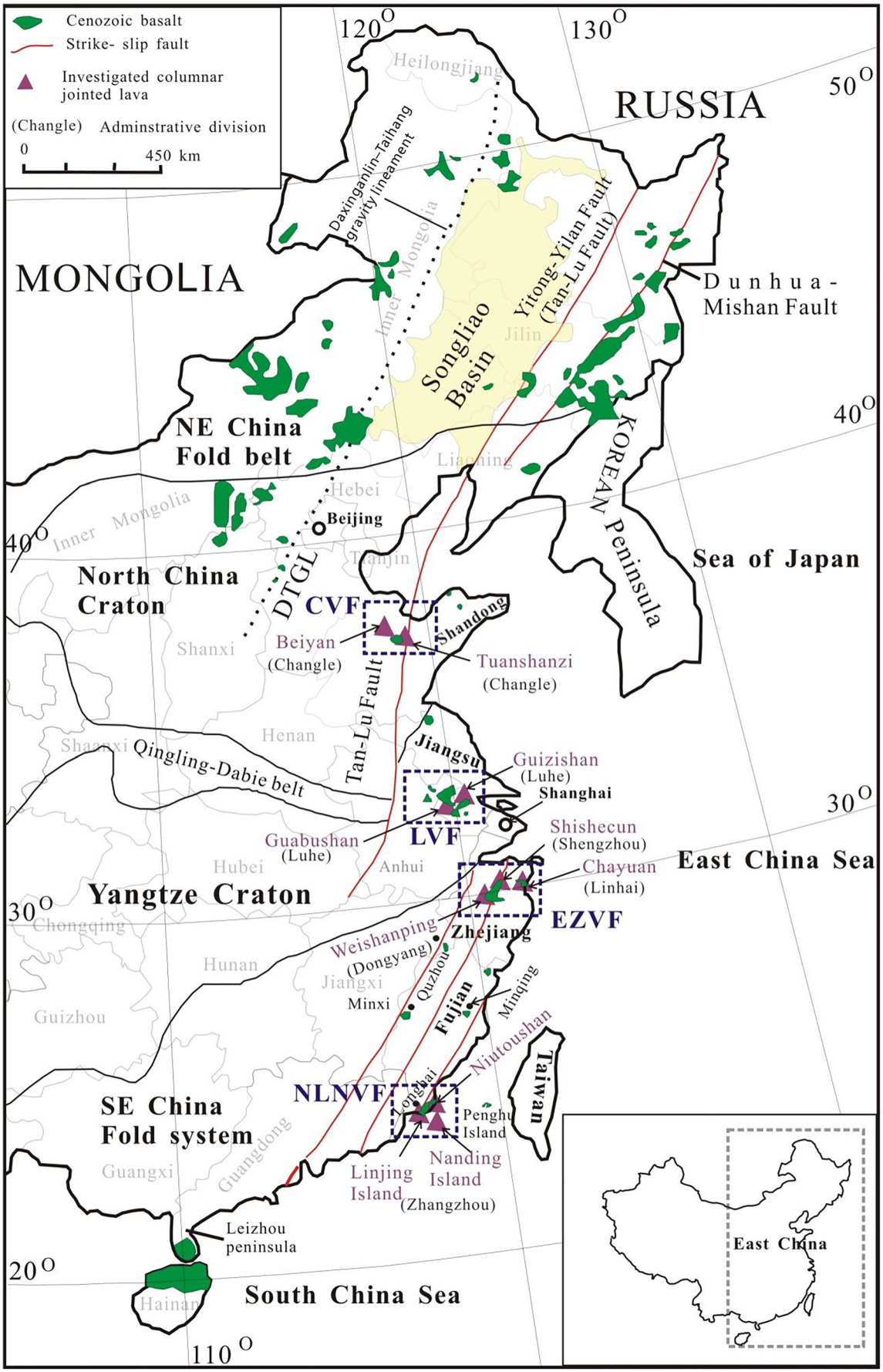
Cenozoic basalt
Strike- slip fault
Investigated columnar jointed lava
(Changle) Adminstrative division
0
450 km
120°
130°
50°
40°
30°
20°
110°
RUSSIA
MONGOLIA
Heilongjiang
Daxinganlin-Taihang gravity lineament
Inner Mongolia
Songliao Basin
Yitong-Yilan Fault (Tan-Lu Fault)
Dunhua-Mishan Fault
Jilin
NE China Fold belt
Liaoning
Hebei
Beijing
Tianjin
KOREAN Peninsula
Sea of Japan
North China Craton
DTGL
CVF
Shandong
Beiyan (Changle)
Tuanshanzi (Changle)
Shanxi
Tan-Lu Fault
Henan
Jiangsu
Guizishan (Luhe)
Shanghai
Qingling-Dabie belt
LVF
Guabushan (Luhe)
Shishecun (Shengzhou)
East China Sea
Hubei
Anhui
Chayuan (Linhai)
Yangtze Craton
EZVF
Chongqing
Weishanping (Dongyang)
Zhejiang
Hunan
Jiangxi
Quzhou
Minxi
Fujian
Minqing
Guizhou
Niutoushan
Taiwan
NLNVF
Longhai
Penghu Island
SE China Fold system
Guangdong
Guangxi
Linjing Island
Nanding Island (Zhangzhou)
Leizhou peninsula
Hainan
South China Sea
East China

Field observations

The EZVF lavas are represented by single EUs, whereas most columnar-jointed lavas in the CVF, LVF, and NLNVF are multiple-unit sequences. Descriptions of the geological features of each of the four volcanic fields are given in Table 2, and geometrical measurements of the columnar jointing are given in Table 3. A total of 49 sites were measured and photographed, and > 3000 side lengths were measured.

Changle volcanic field

Lavas in the Beiyan volcano (BV) of the CVF can be generally divided into two EUs based on their contact relationship. BV-EU1 shows a fanning-downward colonnade (Fig. 3a, b), while BV-EU2 commonly shows inclined and vertical columns (Fig. 3c, d). The two units are not traceable over long distances because of the Quaternary sediment cover and are only visible in quarry sections. There are many types of xenoliths in BV-EU2, including peridotite, pyroxenite, and sapphire (Fig. A1). An outcrop at Tuanshanzi volcano (TV) of the CVF was also examined, revealing two volcanic units, the first being a lava flow with fanning-downward shaped columns (Fig. 4a) and second being a pyroclastic deposit (with bombs and lapilli) (Fig. 4b).

Luhe volcanic field

The Guabushan volcano (GBV) in the LVF exhibits diverse column patterns (Table 2, Fig. 5a). Five types of columnar jointing are observed: inclined, vertical, horizontal, fanning downwards, and fanning upwards (Fig. 5b–g). Two effusive units can be discriminated with an E-W orientation (Fig. 5a). GBV-EU1 is about 30 m thick and has a slightly inclined colonnade, with column diameters of 30–50 cm (Fig. 5b). GBV-EU2 is the main columnar unit (Fig. 5a), is about 60 m thick, and also shows horizontal (Fig. 5c) and basin-pattern colonnades (Fig. 5f; Spry 1962). The columns on the south side are wider (~ 20–30 cm) than those on the north side (~ 10–20 cm).

Columnar joints also occur in the lava flows of Guizishan volcano (GZV) in the LVF (Fig. A2), where there are three types (inclined, vertical, and horizontal), with column diameters of 20–30 cm. The two units can be defined as a lowermost unit with a horizontal shaped pattern of columns (GZV-EU1) and an upper unit with vertical or inclined columns (GZV-EU2). The second unit is about 50 m thick and comprises the major part of the lava section in this volcano.

Eastern Zhejiang volcanic field

Three locations, Chayuan lava in Ninghai, Shishecun lava in Shengzhou, and Weishanping lava in Dongyang (Table 2), were investigated. These lavas are typically single units, with relatively large-diameter (> 50 cm) colonnades.

Columnar joints in the Chayuan lava can be divided into two tiers: a vertical colonnade in the lower part and an entablature in the upper part (Fig. 6a). The entablature is highly brecciated (Fig. 6b). The sides of the columns in the colonnaded tier exhibit horizontal banding with well-formed chisel marks or striae (Fig. 6c), each stria having been formed by the propagation of a crack in the elastic part of the cooling flow (James 1920; Tomkeieff 1940; Spry 1962; Ryan and Sammis 1978; DeGraff and Aydin 1987; Piombo and Dragoni 2018). Most of the cyclic striae are composed of smooth and rough zones with heights of ~ 5–10 cm (Fig. 6d). Also observed are fracture lances (radially oriented platelets surrounding fracture surfaces; Sommer 1969; Ryan and Sammis 1978) on the side faces of columns (Fig. 6c, d), and radial striae similar to plumose markings are observed on column cross sections (Fig. 6e).

In the Shishecun lava, two types of columnar joints (vertical and inclined) occur. Vertical colonnades usually exhibit a regular hexagonal or pentagonal jointing style in the lower part, and the column diameter is > 50 cm (Fig. A3a–d). Instead, the small inclined or curved colonnades are mainly distributed on the upper part of the unit and have the features of entablature.

The Weishanping lava has the form of a lava mesa with very low angles of plunge to the columns (< 10°). Columnar joints exhibit inclined or curved patterns at the margin and top of the mesa and possibly a vertical pattern in the center (Fig. A3e, f).

Niutoushan-Linjin Island-Nanding Island volcanic field

Volcanic cones and flat-lying lava landforms (Fig. A4) are the two main morphologies in the NLNVF. Investigations are focused primarily on the well-exposed lava sections in the Niutoushan, Linjin Island, and Nanding Island (Figs. 7, 8, and 9).

Niutoushan lavas

The NLNVF lavas in Niutoushan area are of three morphological types: (i) vesicular and amygdaloidal basalts with high vesicle contents at the base, gradually changing into (ii) blocky basalt with less vesicles above, in turn overlain by (iii) columnar-jointed pāhoehoe sheet flows (Fig. 7). The outcrop area of the NLNVF is relatively small (< 10 km^2). However, much of the outcrop is underwater, making estimation of total coverage difficult.

In the Niutoushan area, we observed both compound and sheet pāhoehoe flows (Walker 1972; Self et al. 1998). The compound flows are subdivisible into distinct smaller and

Table 2 Summarized characteristics and interpretations of columnar-jointed basaltic lavas in eastern and southeastern China

Volcanic field (area)	Volcano (administrative division)	Central latitude/ longitude	*D* (cm)/*H* (m)	Period (Ma)	Petrology	Characteristics	Interpretation
CVF (~400 km^2)[a]	Beiyan (Changle)	36° 33′ 18″ N/11-8° 47′ 45″ E	~20–30/~10–40	~18.7–18.4[b]	Basanite and alkaline basalt, with a large amount of xenoliths	MUF (2 units), 3 types of columnar joints BV-EU1 shows fanning downward, and BV-EU2 shows vertical/inclined and contains many peridotite, pyroxenite, and sapphire xenoliths, which obviously lack of entablature and interbedded sedimentary layer	An interval period of the 2-unit flows is very transient. Lavas flowed in a relatively dry environment and have undergone a fast cooling process
	Tuanshanzi (Changle)	36° 32′ 31″ N/11-8° 53′ 00″ E	~30–40/~10		Alkaline basalt and/or tholeiite	SUF, a fanning-downward columnar joint, obviously lack of entablature	Lavas flowed in a relatively dry environment and have undergone a relatively slower cooling process
LVF (~726 km^2)[c]	Guabushan (Luhe)	32° 15′ 14″ N/11-8° 53′ 33″ E	~10–50/~40	~9.35[d]	Alkaline basalt and/or tholeiite	MUF (2 units) GBV-EU1 shows relatively regular shape and large size, and GBV-EU2 is the main columnar unit with 5 column patterns	GBV-EU1 underwent a relatively slower cooling process, and GBV-EU2 possibly experienced faster cooling process with the ingress of surface water into solidifying lavas
	Guizishan (Luhe)	32° 27′ 43″ N/11-8° 55′ 59″ E	~30–40/~70		Basanite with large quantities of mantle xenoliths	MUF, 3 types of columnar joints and contain many mantle xenoliths	GZV-EU1 formed by a faster cooling process with the ingress of meteoric water during emplacement, and GZV-EU2 underwent a slower cooling process
EZVF (~700 km^2)[c]	Chayuan (Ninghai)	29° 18′ 57″ N/12-1° 33′ 55″ E	~50–60/~50	~10.5[e]	Quartz tholeiite	SUF, a vertical columnar joint with entablature on top Large-sized column, striae, or chisel marks on the side surface	Heavy rain or injection of subground water during lava flow Large-sized column and striae or chisel marks on the side surface indicate lavas here have undergone a slow cooling process
	Shishecun (Shengzhou)	29° 42′ 43″ N/12-0° 51′ 44″ E	~50–60/~50	~10.5[e]	Olivine tholeiite	SUF, 2 types of columnar joint, probably exist entablature on their top and only remain some remnants	Formed in a relatively wet environment and has undergone slow cooling process
	Weishanping (Dongyang)	29° 19′ 31″ N/12-0° 26′ 45″ E	~30–40/~150		Olivine basalt	SUF, 2 types of columnar joint	Experienced a normal cooling process
NLNVF (>10 km^2)	Niutoushan (Zhangzhou)	24° 13′ 14″ N/11-8° 02′ 27″ E	~30–50/~50	~17.1–11.7[e]	Tholeiite and olivine basalt with large quantities of mantle xenoliths, alkaline basalt	MUF (3 units) N-EU1 lavas are compound flow as vesicular basalt, containing gas vents and pipes. N-EU2 lavas are sheet flow and formed columnar-jointed basalts. N-EU3 lavas contain many mantle xenoliths and obviously lack of entablature	N-EU1 lavas flowed onto wet lands with low effusive rates. N-EU2 lavas erupted as relatively high effusive rates and underwent normally cooling process. N-EU3 lavas flowed in a relatively dry environment. Effusive lavas are successively without or with short interval times between different lava units

Table 2 (continued)

Volcanic field (area)	Volcano (administrative division)	Central latitude/ longitude	*D* (cm)/*H* (m)	Period (Ma)	Petrology	Characteristics	Interpretation
	Linjin Island (Zhangzhou)	24° 11′ 22″ N/11-8° 01′ 23″ E	~20–30/~70		Olivine basalt, alkaline basalt	MUF (2 units) L-EU1 lavas are compound flow, containing gas vents and pipes. L-EU2 lavas are sheet flow and formed columnar-jointed basalts, generally present vertical and inclined columnar joints	L-EU1 is a compound flow that flowed onto wet land with low effusive rates. L-EU2 is sheet lava flowed in a relatively dry environment and without or with short interval periods between 2 lava units
	Nanding Island (Zhangzhou)	24° 08′ 08″ N/11-8° 02′ 19″ E	~15–30/~50		Olivine basalt, alkaline basalt	SUF, lavas are sheet flow and formed columnar-jointed basalts; vesicle zones only occur in the upper part	Lavas flowed in a relatively dry environment

D is the diameter of cross face of columns, and *H* is the height of colonnade in vertical direction

CVF Changle volcanic field, *LVF* Luhe volcanic field, *EZVF* eastern Zhejiang volcanic field, *NLNVF* Niutoushan-Linjin Island-Nanding Island volcanic field, *MUF* multiple-unit flow, *SUF* single-unit flow, *EU* eruptive unit, *BV* Beiyan volcano, *GBV* Guabushan volcano, *GZV* Guizishan volcano, *N* Niutoushan, *L* Linjin Island

[a] Chen et al. (2016)

[b] Chen and Peng (1995) and Du et al. (2009)

[c] Chen et al. (2014)

[d] Chen and Peng (1988)

[e] Ho et al. (2003)

Table 3 Geometry measurements of columnar jointing at four volcanic fields in eastern and southeastern China (see Fig. 1 and Table 2 for locations; Figs. A5–A12 provide raw measurement data)

Location/no.	Shape	*L* (cm)	SD (cm)	*L*[a]	*A* (cm^2)	*D* (number of polygons/m^2)	Number of 4-/5-/6-/7-/8-sided polygons	Average *N*	*Xn*
CVF									
Beiyan-1	Vertical	11	4	98	286	35	0/3/20/3/0	6.0	0.48
Beiyan-2	Vertical	13	3	50	323	31	1/8/14/2/0	5.7	0.75
Beiyan-3	Vertical	10	4	152	286	35	0/11/28/4/0	5.8	0.59
Beiyan-4	Vertical	12	5	88	313	32	2/3/13/4/0	5.9	0.83
Beiyan-5	Vertical	11	4	110	333	30	0/7/18/3/1	5.9	0.69
Beiyan-6	Vertical	11	4	50	345	29	0/5/14/2/1	6.0	0.71
Beiyan-7	Vertical	10	4	53	250	40	0/12/18/5/1	5.9	0.76
Beiyan-8	Vertical	9	2	43	313	32	0/6/12/1/0	5.5	0.61
Beiyan-9	Vertical	11	4	55	227	44	1/2/7/2/0	5.8	0.82
Tuanshanzi-1	Fanning	16	5	145	833	12	10/15/6/0/0	4.8	1.33
LVF									
Guabushan-1	Vertical	23	6	36	1111	9	4/4/0/0/0	4.5	1.58
Guabushan-2	Inclined	23	5	41	1111	9	5/3/1/0/0	4.6	1.60
Guabushan-3	Vertical	27	7	67			Only side measurement		
Guabushan-4	Horizontal	6	3	77	91	110	4/17/5/1/0	5.1	1.12
Guabushan-5	Horizontal	8	3	194	111	90	9/24/16/4/4	5.5	1.18
Guabushan-6	Vertical	7	3	66	179	56	0/8/9/3/0	5.8	0.74
Guabushan-7	Inclined	13	4	44	313	32	0/9/2/0/0	5.2	0.90
Guabushan-8	Horizontal	8	2	41	208	48	0/4/7/0/0	5.6	0.60
Guabushan-9	Horizontal	8	3	55	192	52	3/8/3/1/0	5.1	1.18
Guabushan-10	Horizontal	9	4	100	161	62	10/30/11/2/1	5.1	1.19
Guizishan-1	Inclined	27	8	86	625	16	3/10/4/0/0	5.0	1.14
Guizishan-2	Inclined	16	6	54	714	14	3/6/4/0/0	5.0	1.18
Guizishan-3	Inclined	16	5	55	769	13	3/4/6/1/0	5.4	1.10
Guizishan-4	Inclined	30	9	21	1250	8	3/5/0/0/0	4.6	1.46
EZVF									
Chayuan-1	Vertical	37	8	17			Only side measurement		
Chayuan-2	Vertical	42	10	14			Only side measurement		
Chayuan-3	Vertical	40	13	52			Only side measurement		
Chayuan-4	Vertical	34	10	100	2500	4	1/12/7/0/0	5.3	0.89
Shishecun-1	Inclined	33	12	70			Only side measurement		
Shishecun-2	Vertical	39	13	79			Only side measurement		
Shishecun-3	Vertical	39	14	165	2500	4	0/12/13/4/0	5.7	0.74
NLNVF									
Niutoushan-1	Vertical	18	5	28	1000	10	0/3/6/1/0	5.9	0.63
Niutoushan-2	Vertical	19	6	34	999	11	1/2/7/1/0	6.1	0.80
Niutoushan-3	Vertical	18	7	38	833	12	0/3/8/1/0	5.8	0.58
Niutoushan-4	Inclined	14	4	37	500	20	0/2/12/3/0	6.1	0.54
Niutoushan-5	Inclined	16	6	46	625	16	0/4/10/0/0	5.7	0.53
Niutoushan-6	Inclined	14	5	69	455	22	1/5/15/1/0	5.7	0.67
Nanding-1	Vertical	14	5	143	400	25	1/14/30/4/0	5.8	0.67
Nanding-2	Vertical	12	4	117	323	31	2/10/14/1/0	5.3	0.84
Nanding-3	Vertical	11	6	124	256	39	2/7/21/4/2	5.9	0.87
Nanding-4	Vertical	12	4	81	313	32	0/5/23/2/0	5.9	0.48
Nanding-5	Vertical	13	5	56	345	29	0/13/12/1/0	5.6	0.73

L is the average length of column side, SD is the standard deviation of side length, *A* is the mean area, average *N* is the side number of column at one site, *D* is the number of columns in a square meter, and *Xn* is the hexagonality index

[a] The total number of measurements at one site

thinner flow units, while the sheet flows form thick and extensive layers. The boundaries between successive flows of this kind can be identified by notably more vesicular flow tops and bottoms, following the vesicle structure expected, and defined, for a pāhoehoe lobe by Wilmoth and Walker (1993). In the Niutoushan area, N-EU1 is a relatively thin (< 10 m thick) compound flow, while N-EU2 (> 30 m thick) and N-EU3 (~ 10–20 m thick) are sheet flows with spectacular colonnade (Fig. 7a).

Compound flow units in the Niutoushan area can be distinguished by their "vesicularity" (Fig. 7b). In all the limits of the Niutoushan area, units are relatively dense. Instead, the compound flows are usually more vesicular and amygdaloidal textures (Fig. 7a). There are some gas vents with circular or irregular shapes and diameters of 0.5~2 m. These depressions (Fig. 7c) may be the tops of volatile release channels (Sheth et al. 2017a, b). There are also many gas pipes located west of Niutoushan (Fig. 7d), forming ~ 0.5–1-m-high, irregular, or

Table 4 Major concentrations (wt%) of columnar jointed lavas in eastern and southeastern China

Volcanic field	Lava	Sample no.	Rock type	SiO_2	TiO_2	Al_2O_3	Fe_2O_3T	MnO	MgO	CaO	Na_2O	K_2O	P_2O_5	LOI	Total	Ref.[a]
CVF		07CL07	Alkaline basalt	47.58	1.89	13.91	12.17	0.17	9.27	8.08	2.91	1.24	0.37	2.23	99.82	1
		07CL10	Alkaline basalt	45.68	2.23	13.29	12.93	0.17	10.91	8.18	2.44	1.49	0.37	2.12	99.81	1
		07CL11	Alkaline basalt	45.79	2.52	13.3	13.01	0.18	9.21	8.23	2.61	1.48	0.42	2.95	99.69	1
		07CL13	Alkaline basalt	44.94	2.17	12.84	12.93	0.17	11.82	8.15	2.22	1.47	0.35	2.61	99.67	1
		07CL08	Basanite	42.91	2.89	13.38	14.23	0.2	9.69	9.04	4.75	0.88	0.73	1.47	100.16	1
		07CL09	Basanite	42.14	2.7	13.6	13.19	0.22	9.03	8.66	4.76	2.19	1.07	2.09	99.65	1
		SD1508	Basanite	41.89	2.74	12.79	13.01	0.18	10.83	9.85	3.95	1.92	0.87		98.02	2
		SD1508-2	Basanite	41.94	2.75	12.86	13.04	0.19	10.87	9.96	3.91	1.93	0.87		98.3	2
LVF	Guabushan	LHG-1	Alkaline basalt	47.95	2.2	14.9	9.89	0.15	8.36	7.86	3.06	2.2	0.56		99.92	3
		LHG-2	Alkaline basalt	48.07	2.22	15.1	9.91	0.15	8.19	8.04	3.46	2.52	0.57		99.85	3
	Guizishan	12GZ06-2	Basanite	43.04	2.1	11.51	12.58	0.18	10.69	9.82	4.3	1.4	0.97	1.61	98.2	4
EZVF	Chayuan	CY-1	Quartz tholeiite	50.53	2.97	13.14	11.58	0.14	6.56	9.31	2.81	1.04	0.42	1.33	99.82	New
		CY-2	Quartz tholeiite	50.23	3.17	13.04	11.99	0.15	6.41	9.24	2.7	0.99	0.45	1.45	99.81	New
		CY-4	Quartz tholeiite	50.41	3.19	13.09	11.79	0.14	6.59	9.24	2.91	1.06	0.46	0.94	99.81	New
		CY-6	Quartz tholeiite	50.53	3.21	13.01	12.1	0.15	6.23	8.96	2.7	1.25	0.46	1.22	99.81	New
		Z-8	Quartz tholeiite	49.22	2.5	13.62	10.9		8.27	9.05	2.93	1.02	0.43	1.34	99.439	5
		Z-10	Quartz tholeiite	50.19	2.58	13.41	11.14		7.85	9.28	2.86	0.88	0.44	1.31	100.103	5
		Z-11B	Quartz tholeiite	50.79	2.16	13.65	10.65		7.32	9.09	2.85	0.65	0.3	1.69	99.316	5
		Z-6A	Quartz tholeiite	49.47	2.92	13.6	11.86		7.35	9.53	2.92	0.98	0.64	0.7	100.124	5
		Z-7	Quartz tholeiite	50.86	2.66	13.87	11.34		6.85	9.36	2.87	0.84	0.48	0.39	99.674	5
	Shishecun	SSC-1	Olivine tholeiite	50.28	2.28	13.08	10.81	0.18	6.45	8.94	3.6	1.2	0.42	2.58	99.82	New
		SSC-2	Olivine tholeiite	51.16	2.27	13.15	10.57	0.14	7.19	8.65	3.63	1.22	0.42	1.42	99.82	New
		SSC-4	Olivine tholeiite	50.93	2.27	13.1	10.61	0.15	7.2	8.75	3.61	1.21	0.42	1.58	99.83	New
		SSC-5	Olivine tholeiite	50.69	2.28	13.2	10.49	0.14	6.78	8.87	3.55	1.23	0.43	2.18	99.82	New
		Z-23A	Quartz tholeiite	51.99	2.18	14.12	11.24	0.16	6.99	8.78	3.4	1.24	0.39	0.01	100.5	5
		Z-24	Quartz tholeiite	51.23	2.1	13.89	10.86	0.16	7.15	8.94	3.39	1.15	0.38	0.15	99.4	5
		Z-26A	Olivine tholeiite	50.33	2.31	13.53	10.83	0.156	7.44	8.66	3.78	1.5	0.56	0.31	99.406	5
		Z-28B	Olivine tholeiite	49.27	2.86	14.5	10.53	0.154	6.35	8.3	4.13	2.34	0.79	0.42	99.644	5
NLNVF	Niutoushan	1	Quartz tholeiite	52.87	1.31	15.43	9.67	0.114	6.94	9.06	2.73	0.46	0.18		100.14	6
		2	Quartz tholeiite	51.18	1.07	16.56	8.52	0.9	4.85	7.05	2.97	1.35	1.7		100.49	6
		3	Quartz tholeiite	54.63	1.07	17.24	7.97	0.5	3.78	6.45	3.62	1.91	1.8		100.7	6
		F327	Olivine tholeiite	48.92	1.04	15.64	10.56	0.24	5.49	7.25	3.63	2.43	0.601		99.82	7

Table 4 (continued)

Volcanic field	Lava	Sample no.	Rock type	SiO_2	TiO_2	Al_2O_3	Fe_2O_3T	MnO	MgO	CaO	Na_2O	K_2O	P_2O_5	LOI	Total	Ref.[a]
		F338	Quartz tholeiite	52.53	1.48	14.89	10.35	0.162	6.82	9.34	2.31	0.35	0.284		99.66	7
		F321	Olivine tholeiite	49.78	1.42	12.92	9.09	0.22	6.92	9.22	2.75	0.44	0.19		99.7	7
		F327	Quartz tholeiite	53.39	1.32	15.93	9.09	0.22	6.5	9.72	2.39	0.35	0.15		100.03	7
		F333	Quartz tholeiite	51.91	1.31	15.42	8.96	0.16	7.65	6.18	2.55	0.4	0.18		97.42	7
		6	Quartz tholeiite	51.87	1.52	15.18	9.81	0.1	7.12	8.75	2.38	0.46	0.23			8
		7	Olivine tholeiite	50.65	1.07	13.9	12.93	0.23	6.99	9.46	1.91	0.19	0.14			8
		8	Quartz tholeiite	53.39	1.32	15.93	9.09	0.22	6.5	9.72	2.39	0.35	0.15			8
		9	Olivine tholeiite	50.6	1.44	15.28	11.35	0.19	7.44	9.3	2.92	0.49	0.1			8
		F14B	Quartz tholeiite	52.13	1.95	15.41	9.96	0.128	5.09	7.75	3.24	1.61	0.54		99.608	5
		F-18A	Olivine tholeiite	52.09	1.97	15.21	9.89	0.129	6.46	7.32	3.24	2.04	0.52		99.409	5
		F-20	Olivine tholeiite	49.15	2	14.6	10.27	0.137	7.77	8.61	2.88	1.8	0.43		99.847	5
		F-22	Quartz tholeiite	53.6	1.21	15.38	9.17	0.121	7.11	8.02	2.71	0.64	0.19		99.511	5
		F-24	Olivine tholeiite	50.01	2.12	15.31	9.98	0.122	6.43	7.57	3.55	2.54	0.59		99.742	5
		F-28	Quartz tholeiite	53.74	1.2	15.89	8.99	0.129	6.45	9.31	2.58	0.39	0.14		99.479	5
		NT-1	Olivine tholeiite	50.52	1.36	15.81	11.73	0.18	7.57	9.64	2.51	0.31	0.18		99.8	9
		NT-2	Olivine tholeiite	49.9	1.21	15.4	11.35	0.18	9.51	9.43	2.6	0.31	0.17		100.07	9
		NT-13	Olivine tholeiite	51.6	2.15	16.32	10.31	0.1	4.72	7.42	3.44	2.64	0.61		99.34	9
		NT-19	Olivine tholeiite	49.1	2.56	15.09	11.48	0.13	8.48	7.51	2.6	2.11	0.55		99.63	9
		NT-23	Olivine tholeiite	49.2	2.38	15.3	11.4	0.16	8.39	7.27	3.33	2.26	0.56		100.25	9
		NT-25	Quartz tholeiite	50.4	2.23	15.3	11.4	0.16	6.39	7.45	3.43	2.55	0.62		100.21	9
		NT-26	Olivine tholeiite	48.9	2.34	15.03	11.52	0.16	8.69	7.55	3.37	2.12	0.53		100.23	9
		NT-31	Olivine tholeiite	49.1	2.49	15.31	11.42	0.16	8.46	7.49	2.88	2.12	0.56		99.99	9

New data were analyzed by X-ray fluorescence spectroscopy (XRF) (Magix_pro2440) techniques (Fitton 1997) with analytical uncertainties of 5%, samples were crushed in a steel jaw crusher and then powdered to 200 mesh in an agate mill

LOI loss on ignition

[a] References: (1) Xu et al. (2012), (2) Sakuyama et al. (2013), (3) Zhi (1990), (4) Li et al. (2016), (5) Ho et al. (2003), (6) Zhou and Chen (1981), (7) Zhao et al. (2004), (8) Zhang and Lu (1997), (9) Zou et al. (2000)

cylindrical-shaped mounds or bumps, made up of glassy and angular debris (hyaloclastite).

Sheet flows formed the two units (Fig. 7a, b). N-EU2 is tholeiite (Zou et al. 2000; Ho et al. 2003) and generally exhibits diverse patterns of columnar joints (Fig. 7e, f), which usually show blocky structures and dense vesicular zones at their tops. N-EU2 forms the Niutoushan cone and Tianmashan basaltic platform (Fig. A4II, a, b). Columnar joints are mainly found on the southeastern side of Niutoushan cone, and most of them are arranged in a fan shape (Fig. 7e). The colonnade in N-EU2 shows a high-angle inclined pattern, with a blocky structure and high numbers of vesicles in the upper part of the colonnade. Other colonnades show low-angle inclined or horizontal orientations (Fig. 7f). N-EU3 lava is alkaline basalt

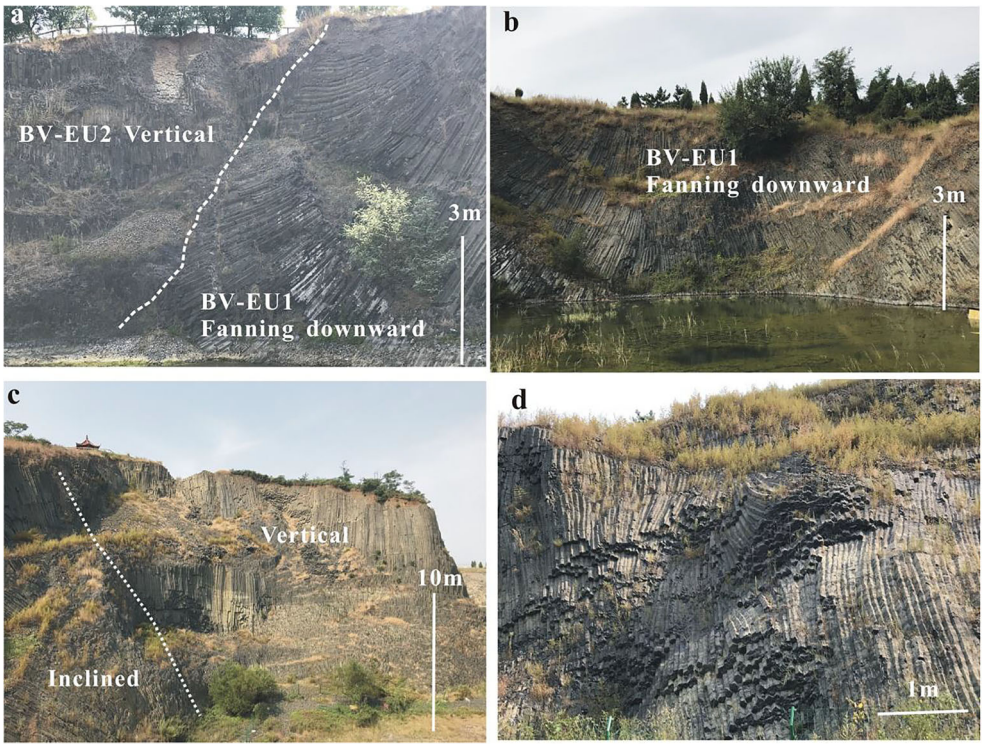

Fig. 3 Different types of columnar joints at Beiyan volcano, CVF. **a** Two sharp contact. **b** BV-EU1 colonnade showing a fanning downward pattern. **c** BV-EU2 colonnade displaying vertical and inclined columnar joints. **d** BV-EU2 colonnade displaying inclined and curved columnar joints

(Zeng et al. 2017) and has a single colonnade. This lava contains large quantities of peridotite xenoliths (~ 5 wt%) which usually have elliptical shapes with diameters of ~ 3–10 cm (Fig. 7g, h). The main columns are six- or five-sided, with a few that are seven- or eight-sided (average side numbers are ~ 5.7–6.1; Table 3). Their side lengths are ~ 14–19 cm, diameters are ~ 28–40 cm, and in a few columns, the diameter can reach > 50 cm.

Linjin Island lava

Linjin Island is about 0.12 km^2 in area (Fig. A4), and the whole island is formed by at least two effusive units (Fig. 8a, b). L-EU1 covers the low parts of the island as a compound flow of vesicular basalt. Gas vents and vesicle cylinders or spiracles occur in this lava unit (Fig. 8c–e). L-EU2 shows blocky structure and forms the exposed base of the lower part and the two-tier colonnades on the upper part (Fig. 8b).

Nanding Island lava

Nanding is a small island (Fig. A4), but famous in China for its spectacularly high colonnade of closely spaced columns. The colonnade in Nanding Island is made up of two-tier structures (Fig. 9a–c). The lower colonnades are generally submerged and usually crops out at the edge of the island, and its uppermost part contains a high content of vesicles (Fig. 9c). The upper colonnade constitutes the bulk of Nanding Island (Fig. 9a). The colonnades of Nanding Island commonly have column diameters of ~ 15–20 cm and column heights of ~ 20–30 m, and the columns are of dense, vesicle-free basalt (Fig. 9d) with high contents of vesicles only in the upper parts. The majority of the columns are regular six- and five-sided at the base (Fig. 9d) and evolving into irregular polygons at the top. Their diameters are notably smaller than those of columns in the Niutoushan area (~ 28–40 cm, Table 2).

Discussion

Previous studies (Tomkeieff 1940; Long and Wood 1986; Lyle 2000; Sheth et al. 2015) considered randomly oriented and thinner (≤ 10 cm) columns as the entablature. The layer typically forms upper tier of a columnar-jointed lava flow and is likely the result of the ingress of surface water into the solidifying lava (Forbes et al. 2014; Sheth et al. 2015). Instead, the colonnade is typically well organized and forms a lower tier (Tomkeieff 1940; Spry 1962). Fanning-downward shaped columns in the Beiyan (Fig. 3c, d) and Tuanshanzi (Fig. 4a) areas of the CVF can therefore be considered as colonnade for the following three reasons. First, fanning-downward columnar joints in the CVF reach > 10 m in height and constitute the whole or most of a lava flow unit (Fig. 4a). Second, there are no other types of structure so the organization is not chaotic (Figs. 3c and 4a). Third, the width of columns generally exceeds 20 cm which is notably larger than the typically thin columns of the entablature (Sheth et al. 2015). We thus suggest that the formation of fanning-downward columns in the CVF is associated with the emplacement within

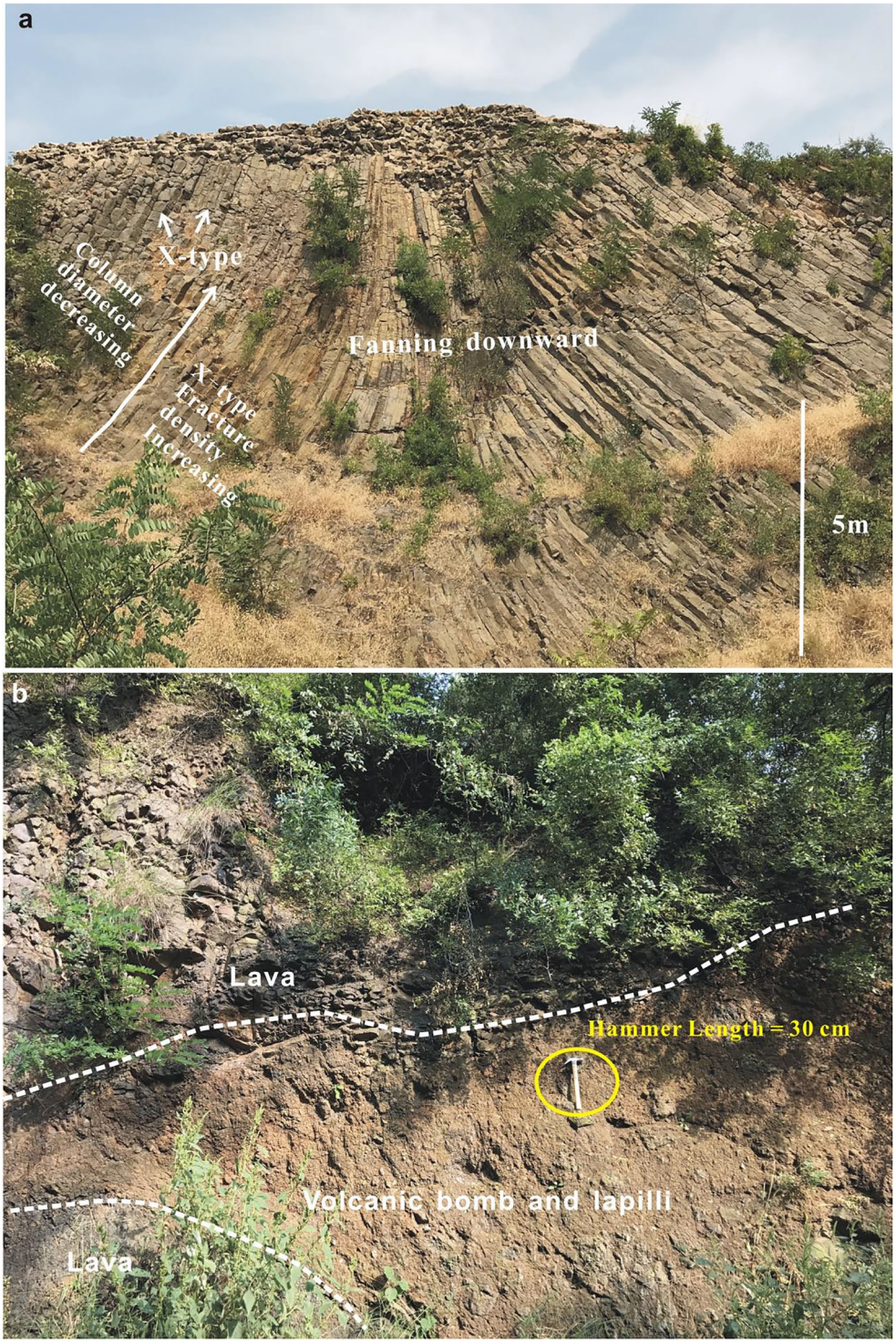

Fig. 4 Lava and volcanic pyroclastic (bomb and lapilli) outcrop at the Tuanshanzi volcano, CVF. **a** Fan-shaped columnar jointing. X-type fractures usually cross-cut flow banding, which are best observed in glass or glassy substances (Forbes et al. 2012), indicating that the upper part of the sequence has undergone a faster cooling. **b** Pyroclastic layer interbedded in lavas; moderately to densely welded deposits indicated that fire fountains occurred during lava flow

confined topography, i.e., within a paleo-valley so that the colonnade fans towards the valley walls.

Entablatures at the Guabushan volcano are horizontal, fanning-downward, and fanning-upward patterns and can therefore be regarded as a classic entablature following the formation processes of Long and Wood (1986) and Lyle (2000). Orientations of the colonnade have a relatively regular pattern that can be regarded as a column-forming entablature. Following Long and Wood (1986), Forbes et al. (2014), and Sheth et al. (2015), such a structure can be ascribed to the ingress of water, possibly heavy rain, but not large quantities of surface water related to flooding during solidification. Horizontal columnar-jointed lavas are found at the lowest levels of the Guizishan volcano. This may indicate a strong

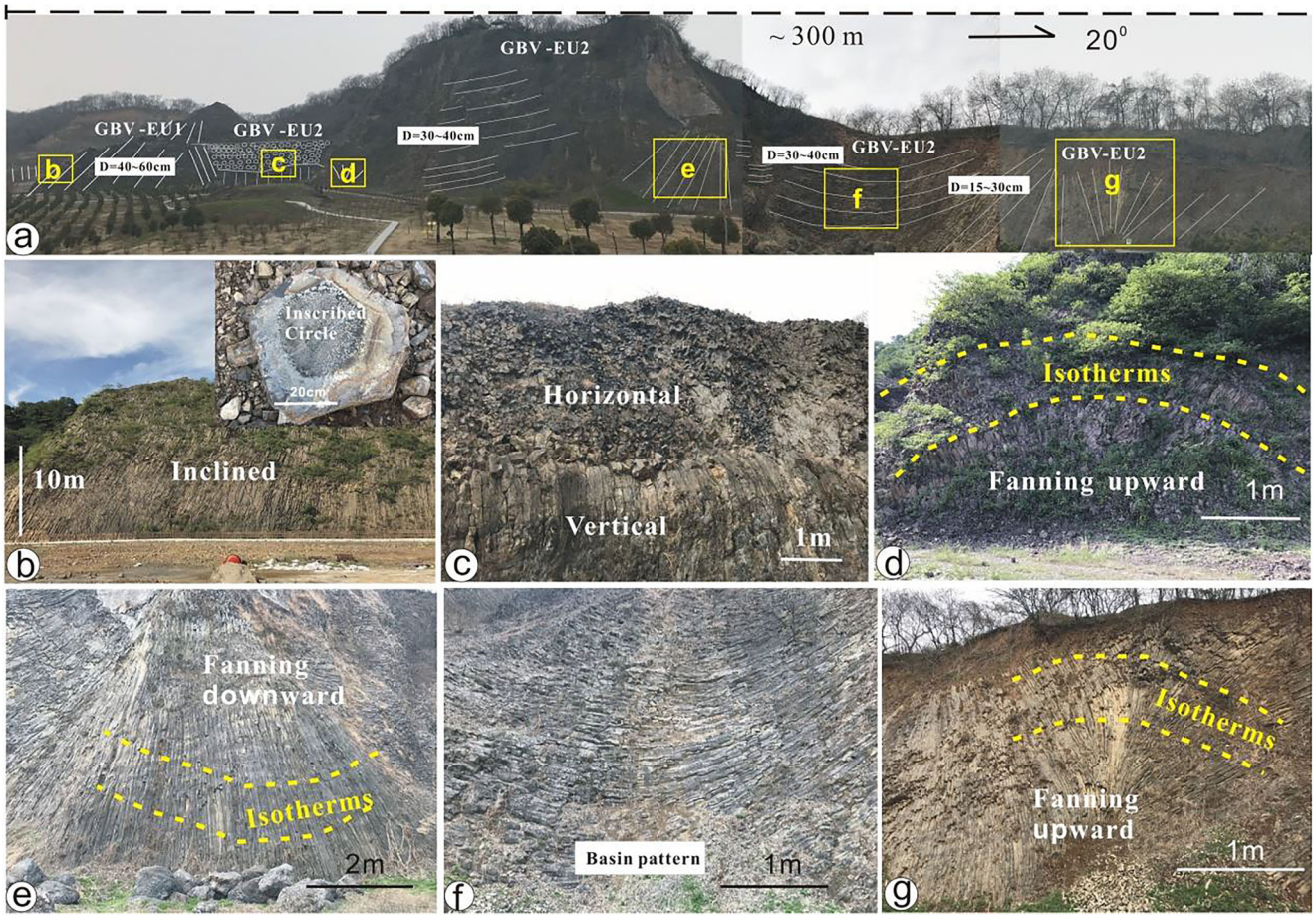

Fig. 5 Different types of columnar joints in the Guabushan area of LVF. **a** A section of a volcanic shield, containing several morphologies; the length of the section is ~300 m, and D = 30~40 cm represents the diameter of a single column. **b** The inclined columnar jointing average of column diameter is ~50 cm. **c** Two-tier structures consisting of horizontal entablature and vertical colonnade. **d** Fanning-upward columnar jointing locates at the lower site. **e** Fanning-downward columnar jointing. **f** A curved columnar jointing. **g** Fanning-upward columnar jointing

local deflection of isotherms due to meteoric water ingress during emplacement of the first lava flows (Long and Wood 1986; Sheth et al. 2015).

Columnar-jointed lava units in the EZVF usually display two-tier structures with an entablature as the upper part and a wide vertical colonnade in the lower part. The wide (~50–80 cm width) columns typical of the EZVF colonnade indicate that lavas here have undergone a slow cooling process (Peck et al. 1966; Peck and Minakami 1968; Wright and Okamura 1977; Harris and Rowland 2009). Entablature in the Chayuan lava units is generally highly brecciated and contains hyaloclastites (Fig. 6b). The formation of these entablatures thus likely resulted from the ingress of large amounts of surface water into solidifying lavas, possibly during a flood event (Lyle 2000; Forbes et al. 2014; Fowler et al. 2014).

The compound lava flows of the Niutoushan area and Linjin Island are highly vesicular, with gas vents and gas pipes. Such structures may result from lavas entering seawater or wet beach sediments, with conversion of the seawater or water trapped within the sediments to steam generating the gas-escape pipes and vents (Philpotts and Lewis 1987; Goff 1996; Reidel et al. 2013; Fowler et al. 2014).

Variable cooling rates based on column size and shape

Early-stage (~17–12 Ma; Chen and Peng 1985; Ho et al. 2003; Du et al. 2009) columnar-jointed basalt outcrops in the CVF and NLNVF have colonnades, but no entablatures above the colonnades. Also, no pillow lavas or hyaloclastites occur at the bases of these colonnades (see Sheth et al. 2015 for good examples). These columnar-jointed basalts thus correspond to the type I flows of Long and Wood (1986), lacking entablatures above colonnades and indicating that the lava flows were emplaced on a dry substrate and formed in a dry condition, so that the colonnades formed slowly by essentially conductive cooling (Long and Wood 1986; Goehring and Morris 2008). In contrast, thick entablatures overlying the colonnades in the late-stage (~11–2.5 Ma; Chen and Peng

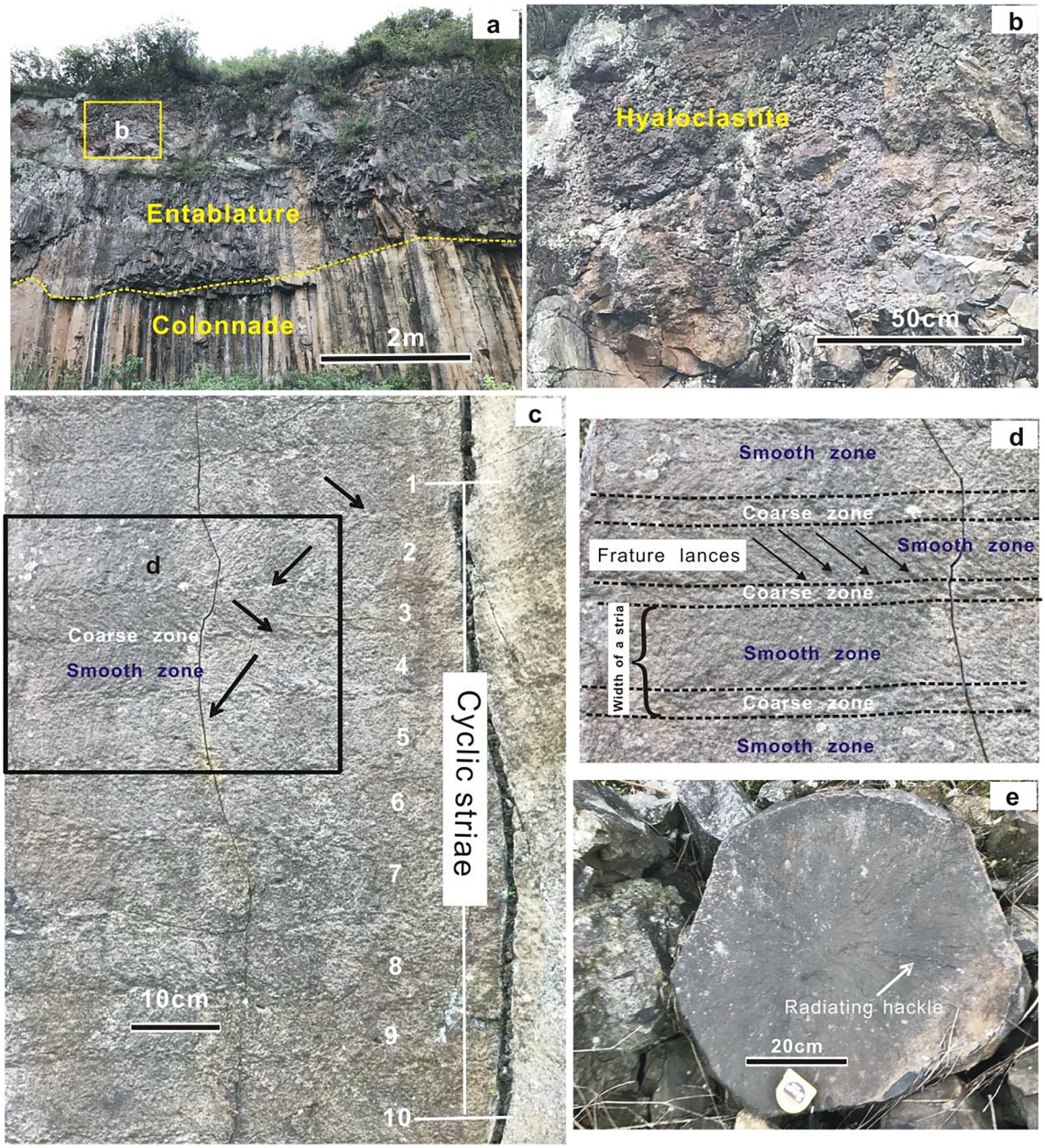

Fig. 6 Morphology of the Chayuan basalt, EZVF. **a** Unit with colonnade and entablature of the upper portions, corresponding to the type III flows of Long (1978). **b** Enlargement of the entablature, which is mainly composed of brecciated basalt. **c**, **d** Cyclic striae and fracture lance on the side surface of column (DeGraff and Aydin 1987); striae spacings are ~ 5–10 cm, equal to ~ 10–20% of column side length, and *arrows* show the direction of fracture lances. Numbers in **c** present 10 striae identified for this case. **e** Radial striae on top surface

1988; Ho et al. 2003) columnar-jointed basalts of the Chayuan (EZVF) and Guabushan (LVF) volcanoes indicate the ingress of meteoric water during solidification of the lava (cf. Lyle 2000; Sheth et al. 2015; Moore 2019).

Column side measurements (Table 3, Figs. A5–A12) show that alkaline basaltic lavas (Zhou and Chen 1981; Sakuyama et al. 2013) in the Beiyan (CVF), Guabushan (LVF), and Nanding Island (NLNVF) areas have slender columns with side lengths of ~ 10–30 cm (Fig. 10a, c, g). Instead, tholeiitic lavas (Li et al. 2015) in the Chayuan and Shishecun areas (EZVF) present larger columns with side lengths of ~ 30–50 cm (Fig. 10e, f). It is interesting to note that tholeiitic lavas (Ho et al. 2003) in the Niutoushan (NLNVF) and alkaline basaltic lavas (Li et al. 2016) in the Guizishan (CVF) have medium-sized columns with widths in the range ~ 10–40 cm (Fig. 10c, h), which is consistent with columnar joint theory where cooling rate, and thus flow thickness, is a primary control on column size (Grossbacher and McDuffie 1995; Goehring and Morris 2008; Hetényi et al. 2012). Thus, thick and basic lavas should form relatively large-sized columnar joints, while thin and felsic lavas may form relatively small-sized colonnades. The results of our measurements strongly

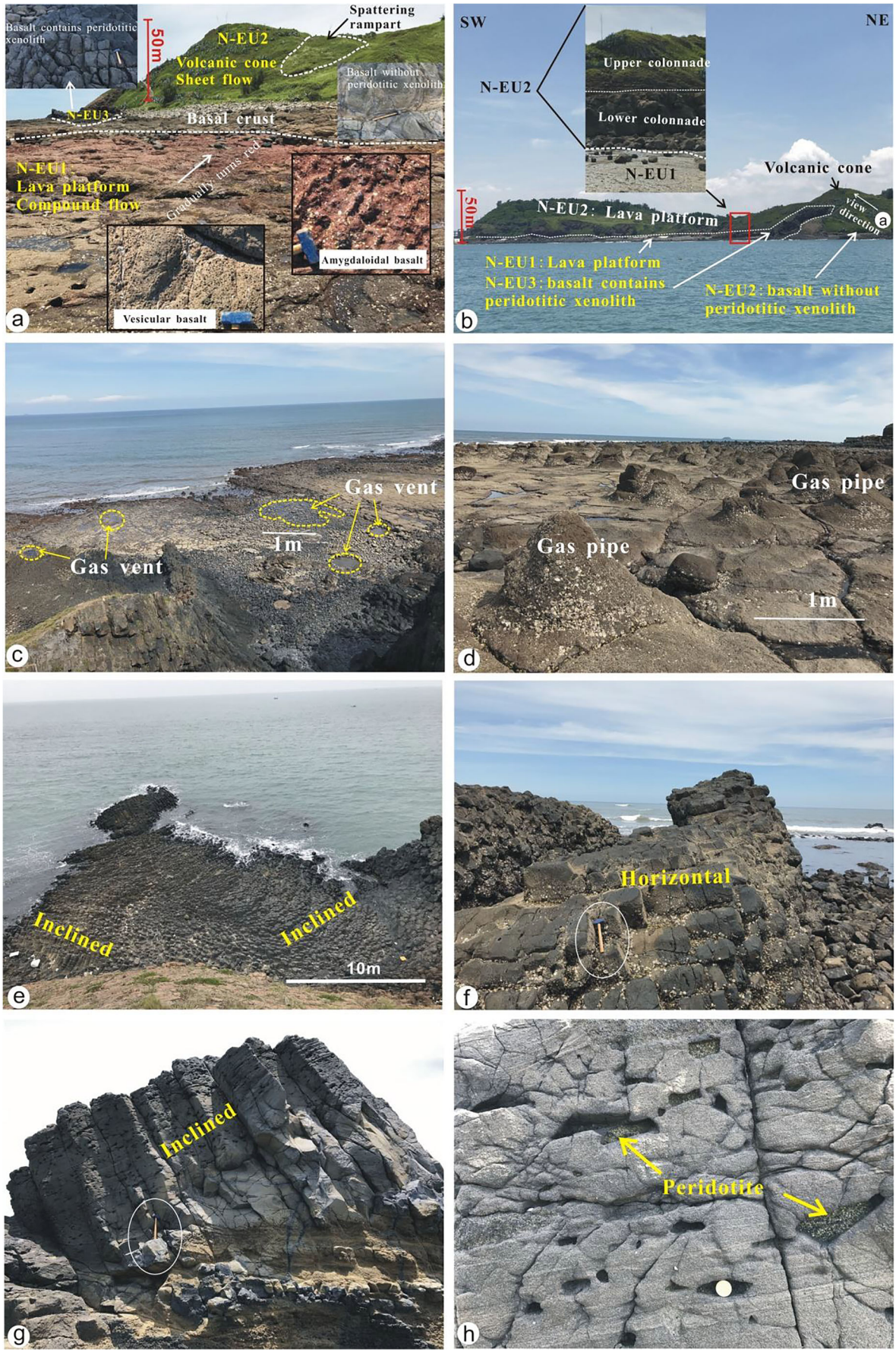
Basalt contains peridotitic xenolith
50m
N-EU2
Volcanic cone
Sheet flow
Spattering rampart
Basalt without peridotitic xenolith
N-EU3
Basal crust
N-EU1
Lava platform
Compound flow
Gradually turns red
Amygdaloidal basalt
Vesicular basalt
a
SW
NE
N-EU2
Upper colonnade
Lower colonnade
N-EU1
Volcanic cone
50m
N-EU2: Lava platform
view direction
a
N-EU1: Lava platform
N-EU3: basalt contains peridotitic xenolith
N-EU2: basalt without peridotitic xenolith
b
Gas vent
Gas vent
1m
c
Gas pipe
Gas pipe
1m
d
Inclined
Inclined
10m
e
Horizontal
f
Inclined
g
Peridotite
h

◀ **Fig. 7** The main morphologies of lavas in the Niutoushan area. **a** Units and morphologies in the east of the area. **b** Units and morphologies in the west of the area. **c** Gas vent expressed as a circular depression. **d** Gas pipe expressed as irregular, cylindrical features with positive relief. **e** Fan-shaped columnar joints (inclined). **f** Colonnade with horizontally oriented columns; hammer (40 cm long) in circle provides a scale. **g** Olivine basalt (N-EU3) with high-angle inclined columns. **h** Peridotite enclaves; coin 2.5 cm in diameter provides a scale

support that chemical composition (Table 4, Fig. A13) and lava unit thickness play the major roles in determining column where felsic and thicker lavas should form larger columns (Hetényi et al. 2012). This relation can also be seen in Guabushan volcano (LVF) where column side lengths (~ 20–30 cm) of GBV-EU1 lava (Fig. 11a, b) are significantly greater than those of GBV-EU2 (side lengths being ~ 5–15 cm) lavas (Fig. 11c–f). Note that GBV-EU1 lavas are more felsic than GBV-EU2 lavas.

As required by minimum-energy considerations (Hetényi et al. 2012), columns should ideally be regular hexagons. However, this ideal is rarely obtained and our field investigations show that these basalts are no different. The maturity of columnar jointing patterns in the four volcanic field areas studied here was statistically analyzed following the hexagonality index of Phillips et al. (2013) (Table 3, Fig.

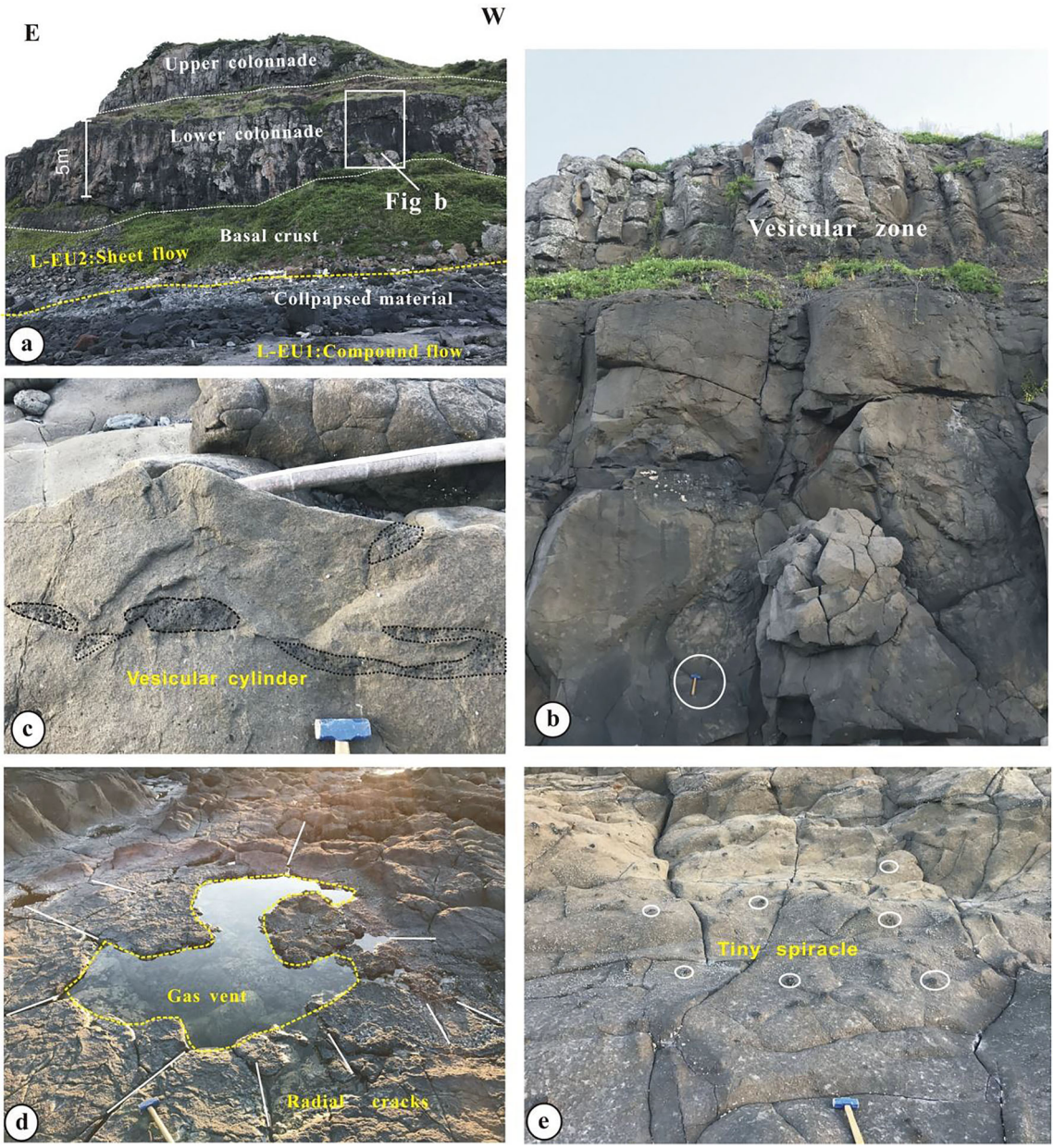

Fig. 8 Lava flow units at Linjin Island, NLNVF. **a**, **b** Two units exhibiting two tiers of colonnade. **c** Interior structure of colonnade, showing horizontally oriented vesicle cylinders. **d** Gas vent with irregular shape and radial cracks. **e** Tiny spiracle on flow surface

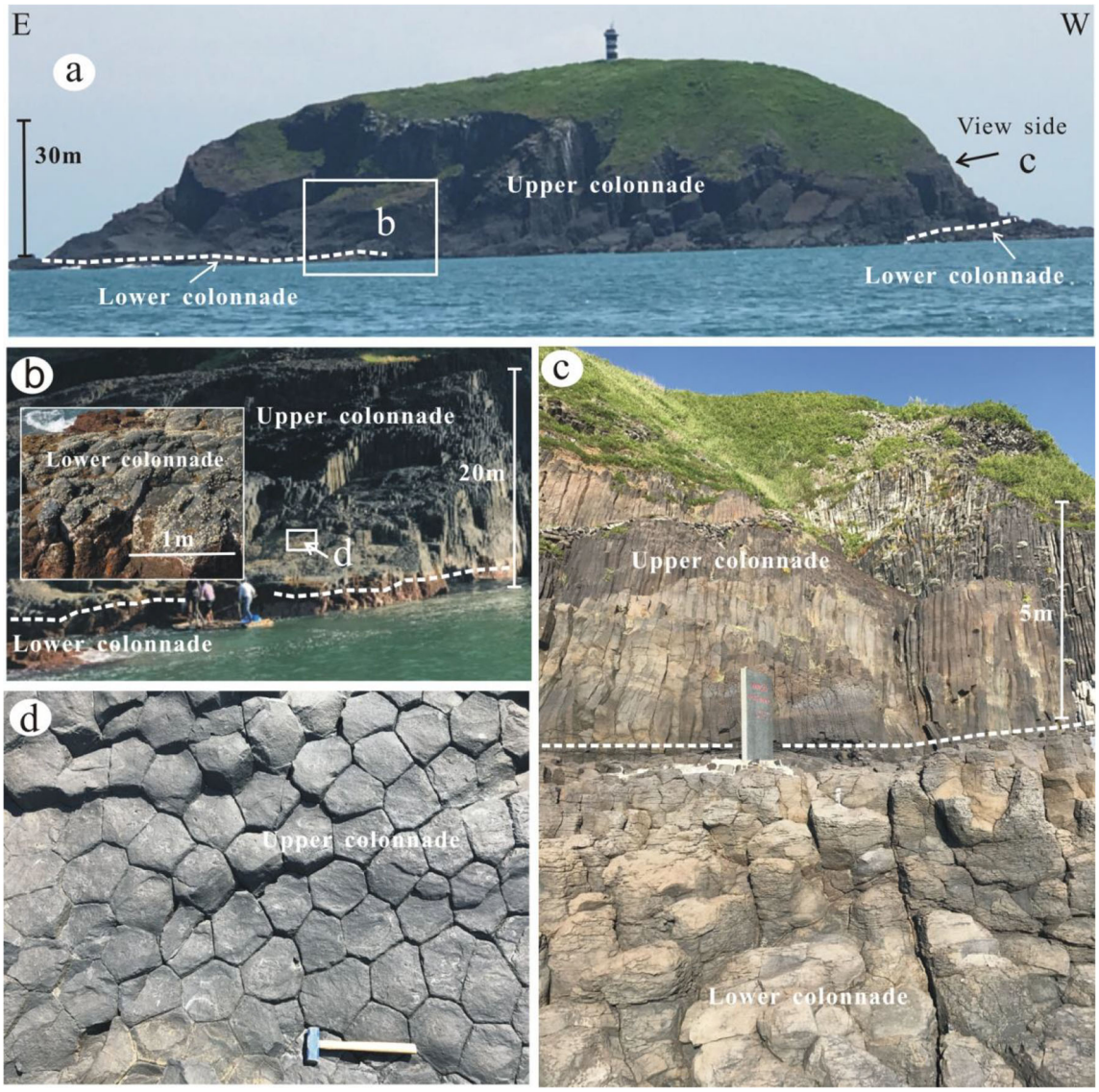

Fig. 9 Morphologies and interior structures of lavas on Nanding Island. **a**–**c** Two-tiered units. **d** Colonnade in the upper tier. The contacts between the upper and lower colonnades are shown by dashed lines

12). Our results indicate that vertical columnar joints in the Beiyan (CVF), EZVF, and NLNVF lava flow units have mature patterns (hexagonality index generally < 1) which are dominated by six, but also comprising of five- and seven-sided columns. This is similar to results from elsewhere in the world, including 0.78–0.8 for the Giant's Causeway (Northern Ireland, UK), 0.92 for the Devils Postpile (California, USA), and 0.79–0.87 for Staffa Island, Scotland (Beard 1959; Phillips et al. 2013). This indicates slow cooling rates in a static lava so as to allow enough time to form mature columnar jointing (Phillips et al. 2013). In contrast, fanning shaped, horizontal, or highly inclined columnar joints in the Tuanshanzi (CVF) and LVF represent immature patterns, with a hexagonality index of generally > 1 and dominated by four-, five-, and seven-sided columns (Fig. 12). Such columnar joints may form on inclined slopes during flow lacking enough time that form regular, vertical columnar joints during faster cooling (Lyle 2000; Forbes et al. 2014; Sheth et al. 2015; Moore 2019). In the Staffa Island basalt, higher hexagonality indexes of 1.2 and 1.1 were found in entablature and hyaloclastite units, respectively. This was interpreted as resulting from a crack pattern consisting of abundant four-, five-, six-, and seven-sided columns, and dominated by five-sided columns (Phillips et al. 2013). We note that small-sized columns ($d < 2$ cm) formed by shrinkage of wet starch usually present a characteristic of more sides (> 6) and higher hexagonality index (> 1) (Fig. 12; Müller 1998b). This is likely due to faster drying, i.e., faster cooling in molten lava. Therefore, vertical or slightly inclined columnar joints usually present relatively well-ordered patterns, most of which are six-sided columns with lower hexagonality indices (< 1), indicating these lavas were emplaced on relatively flat lands or were

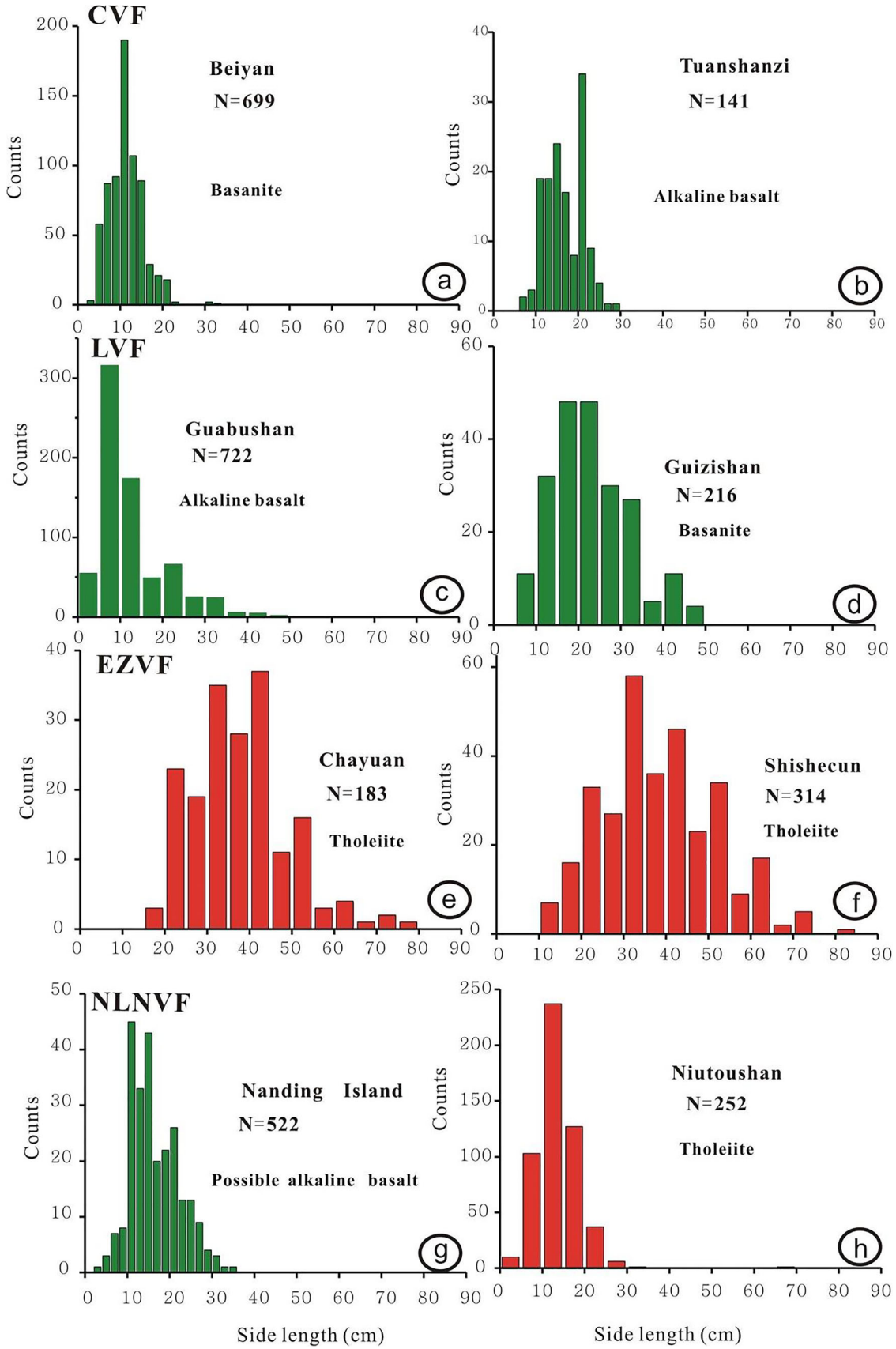

Fig. 10 **a**–**h** Histograms of column side lengths from the four volcanic fields. Data is in Tables 2, 3, and 4

ponded such that the surfaces were nearly horizontal (Waters 1960; Sheth et al. 2015). In contrast, horizontal and fanning shaped columnar joints generally show immature patterns with only few proportions of six-sided column and a hexagonality index of greater than 1. This indicates that these lavas were likely emplaced in a valley so that cooling fronts did not propagate horizontally (Sheth et al. 2015).

A classification of colonnades by orientation

Orientation of columns is a function of isotherm orientation. Thus, the shape of the cooling surfaces will be controlled by the shape of the surrounding topography so the column inclination will reflect the form of the paleotopography. Here, lava flows emplaced on flat surfaces will have vertical columns, those emplaced on sloping surfaces will be inclined, and valley-confined flows will have fanning or horizontal patterns. The slope or degree of confinement will also impact flow thickness, where Hulme (1974) showed that low or no slope results in thicker flows due to yield strength controls on flow spreading. Thicker flows will cool more slowly (Hetényi et al. 2012) and will thus have time to form more well-developed columns of larger size and lower hexagonality index.

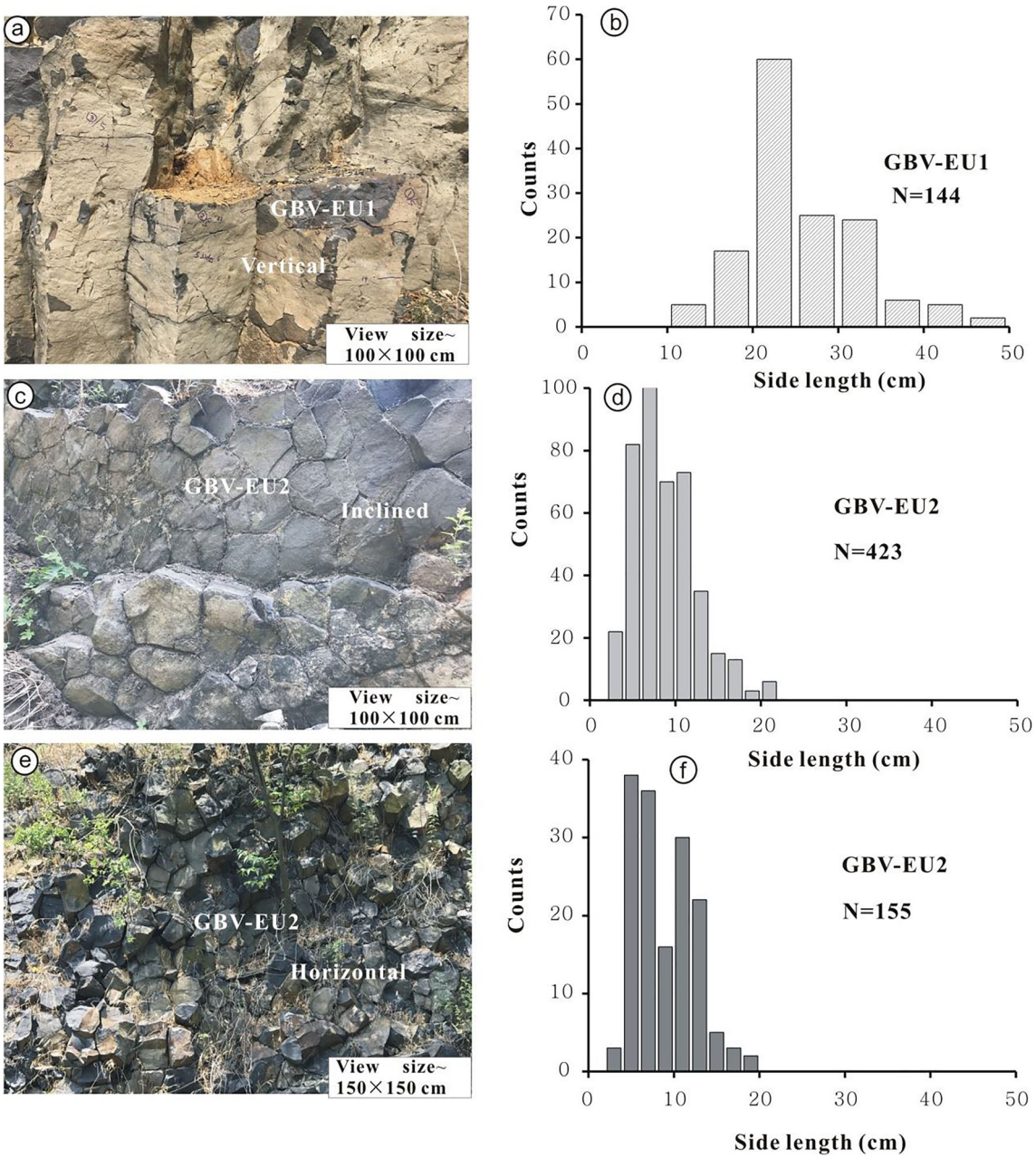

Fig. 11 **a**–**f** Histograms of column side lengths in the Guabushan volcano (LVF), eastern China. Data is in Table 3

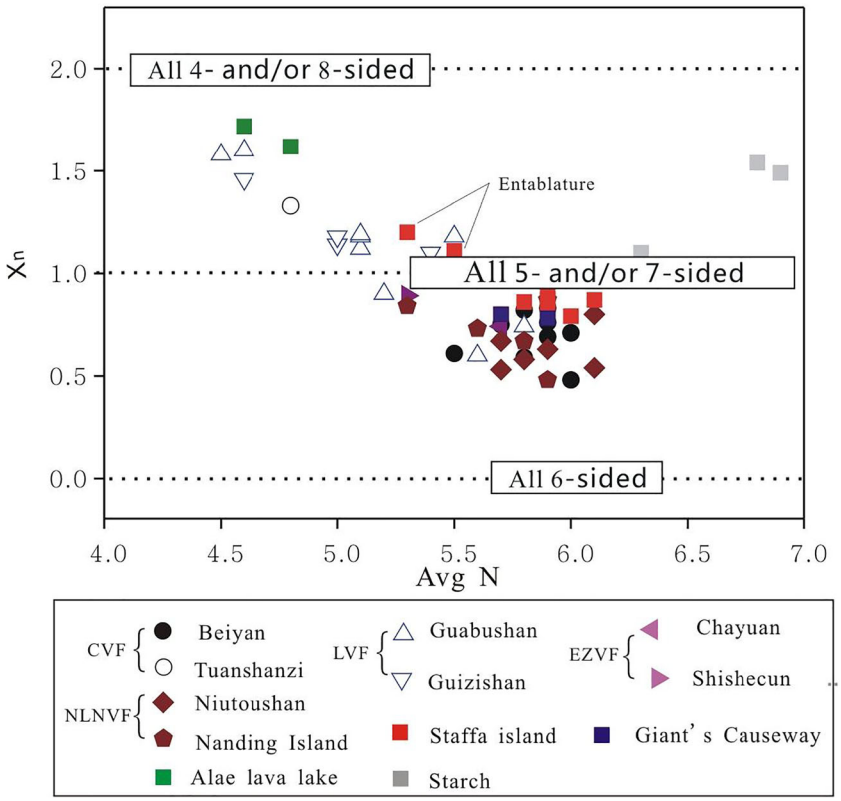

Fig. 12 Hexagonality index (*Xn*) versus average number of sides (Avg *N*). Open symbols represent variable columnar alignment (fanning, horizontal, and inclined), and solid symbols generally present vertical patterns. Data are in Table 3. Other data were from Table 1 in Phillips et al. (2013) and mainly include Saffa Island (Phillips et al. 2013), Giant's Causeway (O'Reilly 1879; Beard 1959), Alae lava lake (Peck and Minakami 1968), and starch (Müller 1998b)

Cooling patterns and rates

Our work suggests a simple qualitative description of different types of colonnade can be made based on their alignment patterns, enabling a classification of colonnades into five types, namely (i) vertical (columns plunge at $\theta > 80°$), (ii) inclined (columns plunge at $10° < \theta < 80°$), (iii) horizontal (columns plunge at $\theta < 10°$), (iv) fanning upwards, and (v) fanning downwards (Fig. 1d–h). This classification allows fast outcrop characterization that may inform on cooling and emplacement history. Because joints develop perpendicular to isotherms during flow cooling (Lyle 2000), the isotherms in the five above types must be (i) subhorizontal, (ii) inclined, (iii) subvertical, (iv) convex-up, and (v) convex-down, respectively (Fig. 1d–h).

It is arguably owing to different cooling rates that horizontal and fanning shaped patterns of the colonnade involve narrower or immature columns (rapid cooling), while slightly inclined and vertical patterns generally involve wider or mature columns (slower cooling). Therefore, by distinguishing the alignment patterns of columns could provide a direct and easy interpretation of the different solidification processes during lava unit cooling.

Conclusions and perspectives

Field observations and interpretations from four volcanic fields in eastern and SE China help us to understand the formation of columnar jointing patterns. The colonnade-bearing flows in the CVF and NLNVF correspond to the type I columnar-jointed lava flows of Long and Wood (1986), lacking overlying entablatures. The columnar-jointed lavas in the LVF usually show five typical jointing patterns (vertical, inclined, horizontal, fanning upwards, and fanning downwards). Instead, vertical colonnades commonly with entablatures in most lavas of the EZVF indicate wet conditions favorable to colonnade formation in these units. The colonnade morphologies are mainly controlled by the paleo-environmental conditions (dry or wet; flat or incised topography), lava thickness, and cooling rate, with the first condition determining the orientation of the cooling front, as well as the formation, or not, of entablature.

The work presented here is a start to the detailed and systematic volcanological studies needed of the volcanic fields of eastern and SE China. As shown here, such an analysis will not only achieve a much better and holistic understanding of the geological evolution of this region but will also inform on the dynamics of volcanic processes, in this case the cooling histories of columnar-jointed lava flows.

Acknowledgments We are grateful to Associate Editor Dr. Dietterich and Executive Editor Dr. Harris for making very insightful comments and suggestions for revising the manuscript. Our thanks also go to Dr. Sheth and an anonymous reviewer, for the excellent detailed comments and suggestions which were very helpful in improving this manuscript.

Funding information This work was supported by the Chinese Academy of Sciences (Project number: XDB01800000).

References

Beard CN (1959) Quantitative study of columnar jointing. Geol Surv Am Bull 70:379–382

Bosshard SA, Mattsson HB, Hetényi G (2012) Origin of internal flow structures in columnar-jointed basalt from Hrepphólar, Iceland: I. Textural and geochemical characterization. Bull Volcanol 74: 1645–1666

Budkewitsch P, Robin PY (1994) Modelling the evolution of columnar joints. J Volcanol Geotherm Res 59:219–239

Bulkeley R (1693) Part of a letter from Sir R.B.S.R.S. to Dr. Lister, concerning the Giants Causway in the county of Atrim in Ireland. Philos Trans R Soc London 17:708–710

Cas RAF, Wright JV (1987) Volcanic successions: modern and ancient. A geological approach to processes, products and successions. Allen and Unwin, London pp. 1–518.

Chen DG, Peng ZC (1985) K-Ar ages and Pb, Sr isotope characteristics of Cenozoic volcanic rocks in Shangdong, China. Geochemica 4:293–303 (in Chinese with English abstract)

Chen DG, Peng ZC (1988) K-Ar ages and Pb, Sr isotope characteristics of some Cenozoic volcanic rocks from Anhui and Jiangsu provinces, China. Acta Petro Sinica 2:3–12 (in Chinese with English abstract)

Chen XY, Chen LH, Chen Y, Zeng G, Liu JQ (2014) Distribution summary of Cenozoic basalts in Central and Eastern China. Geol Journal of China Universities 20:507–519 (in Chinese with English abstract)

Chen S, Li XP, Kong F, Zhao LQ, Chen HK (2016) Mineral characteristics and origin discussion of corundum/sapphire in Cenozoic alkali basalts of the Changle, western Shandong, China. Advances in Geosciences 6:115–128 (in Chinese with English abstract)

Chen H, Xia QK, Ingrin J, Deloule E, Bi Y (2017) Heterogeneous source components of intraplate basalts from NE China induced by the ongoing Pacific slab subduction. Earth Planet Sci Lett 459:208–220

Chung SL, Yang TF, Chen SJ, Chen CH, Lee T, Chen CH (1995) Sr–Nd isotope compositions of high-pressure megacrysts and a lherzite inclusion in alkali basalts from western Taiwan. J. Geol. Soc. China 38(1):15–24

Chung SL, Cheng H, Jahn BM, O'Reilly SY, Zhu B (1997) Major and trace element, and Sr-Nd isotope constraints on the origin of Paleogene volcanism in South China prior to the South China Sea opening. Lithos 40:203–220

DeGraff JM, Aydin A (1987) Surface morphology of columnar joints and its significance to mechanics and direction of joint growth. Geological Society of American 99:605–617

Du SJ, Xu XW, Yang LK, Fu C, Su J, Cui ML (2009) Determining the ending time of basaltic volcanic activity by $^{40}Ar/^{39}Ar$ age of phlogopites from mantle-derived xenolith. Acta Petro Sinica 25:3251–3258 (in Chinese with English abstract)

Fitton G (1997) X-Ray fluorescence spectrometry. In Gill R (ed.), Modern analytical geochemistry: an introduction to quantitative chemical analysis for Earth, environmental and material scientists. Addison Wesley Longman, UK.

Forbes AES, Blake S, McGarvie DW, Tuffen H (2012) Pseudopillow fracture systems in lavas: insights into cooling mechanisms and environments from lava flow fractures. J Volcanol Geotherm Res 245–246:68–80

Forbes AES, Blake S, Tuffen H (2014) Entablature: fracture type and mechanisms. Bull Volcanol 76:820

Fowler AC, Rust AC, Vynnycky M (2014) The formation of vesicular cylinders in pāhoehoe lava flows. Geophys Astrophys Fluid Dyn 109:1–23

Goehring L, Morris SW (2008) Scaling of columnar joints in basalt. J Geophy Res 113:B10203. https://doi.org/10.1029/2007JB005018

Goehring L, Lin Z, Morris SW (2006) An experimental investigation of the scaling of columnar joints. Phys Rev E 74:036115

Goehring L, Mahadevan L, Morris SW (2009) Nonequilibrium scale selection mechanism for columnar jointing. Proc Nat Acad Sci 106(2):387–392

Goff F (1996) Vesicle cylinders in vapor-differentiated basalt flows. J Volcanol Geotherm Res 71:167–185

Grossbacher K, McDuffie SM (1995) Conductive cooling of lava: columnar joint diameter and stria width as function of cooling rate and thermal gradient. J Volcanol Geotherm Res 69:95–103

Guy B (2010) Comments on "Basalt columns: large scale constitutional supercooling?" by John Gilman (JVGR, 2009) and presentation of some new data. J Volcanol Geotherm Res 194:69–73

Harris AJL, Rowland SK (2009) Effusion rate controls on lava flow length and the role of heat loss: a review. In: Hoskuldsson A, Thordarson T, Larsen G, Self S, Rowland S (eds) The legacy of George P.L Walker, Special Publications of IAVCEI 2. Geological Society of London, London, pp 33–51

Hetényi G, Taisne B, Garel F, Médard É, Bosshard S, Mattsson HB (2012) Scales of columnar jointing in igneous rocks: field measurements and controlling factors. Bull Volcanol 74:457–482

Ho KS, Chen JC, Lo CH, Zhao HL (2003) ^{40}Ar-^{39}Ar dating and geochemical characteristics of Late Cenozoic basaltic rocks from the Zhejiang-Fujian region, SE China: eruption ages, magma evolution and petrogenesis. Chem Geol 197:287–318

Hulme G (1974) The interpretation of lava flow morphology. Geophys J R Astron Soc 39:361–383

James AVG (1920) Factors producing columnar structures in lavas and its occurrence near Melbourne, Australia. Journal of Geology 28:458–469

Lamur A, Lavallée Y, Iddon FE, Hornby AJ, Kendrick JE, von Aulock FW, Wadsworth FB (2018) Disclosing the temperature of columnar jointing in lavas. Nat Commun 9(1):1432

Li YQ, Ma CQ, Robinson PT, Zhou Q, Liu ML (2015) Recycling of oceanic crust from a stagnant slab in the mantle transition zone: evidence from Cenozoic continental basalts in Zhejiang Province, SE China. Lithos 230:146–165

Li YQ, Ma CQ, Robinson PT (2016) Petrology and geochemistry of Cenozoic intra-plate basalts in east-central China: constraints on recycling of an oceanic slab in the source region. Lithos 262:27–43

Long PE (1978) Characterization and recognition of intraflow structures. RHO-BWI-LD-IO. Rockwell Hanford Operations, Richland, Grande Ronde Basalt, p 74

Long PE, Wood BJ (1986) Structures, textures, and cooling histories of Columbia River basalt flows. Geol Soc Am Bull 97:1144–1155

Lyle P (2000) The eruption environment of multi-tiered columnar basalt lava flows. J Geol Soc Lond 157:715–722

Mallett R (1875) On the origin and mechanism of production of the prismatic (or columnar) structure of basalt. Proc Roy Soc London 23:180–184

Milazzo MP, Keszthelyi LP, Jaeger WL, Rosiek M, Mattson S, Verba C, Beyer RA, Geissler PE, McEwen AS, HiRISE Team (2009) Discovery of columnar jointing on Mars. Geology 37:171–174

Moore JG (2019) Mini-columns and ghost columns in Columbia River lava. J Volcanol Geotherm Res 374:242–251

Müller G (1998a) Experimental simulation of basalt columns. J Volcanol Geotherm Res 86:93–96

Müller G (1998b) Starch columns: analog model for basalt columns. J Geophys Res 103:15239–15253

Müller G (2001) Experimental simulation of joint joint morphology. J Struct Geol 23:45–49

Nichols RL (1936) Flow-units in basalt. J Geol 44:617–630

Niu ML, Zhu G, Song CZ, Wang DX, Liu GS (2000) Volcanic activities and deep geological processes in the Tan-Lu fault zone. Geol Sci & Tech Info 19:21–26 (in Chinese with English abstract)

O'Reilly JP (1879) Explanatory notes and discussion on the nature of the prismatic forms of a group of columnar basalts, Giant's Causeway. Trans Roy Ir Acad 26:641–728

Peck DL, Minakami T (1968) The formation of columnar joints in the upper part of Kilauean lava lakes. Hawaii Geol Soc Am Bull 79: 1151–1166

Peck DL, Wright TL, Moore JG (1966) Crystallization of tholeiitic basalt in Alae lava lake, Hawaii. Bull Volcanol 29:487–498

Phillips JC, Humphreys MCS, Daniels KA, Brown RJ, Witham F (2013) The formation of columnar joints produced by cooling in basalt at Staffa, Scotland. Bull Volcanol 75:715

Philpotts AR, Lewis CL (1987) Pipe vesicles—an alternative model for their origin. Geology 15:971–974

Piombo A, Dragoni M (2018) A model for crack initiation in solidifying lava. J Geophys Res: Solid Earth 123:8445–8458

Reidel SP, Camp VE, Tolan TL, Martin BS (2013) The Columbia River flood basalt province: stratigraphy, areal extent, volume, and physical volcanology. In: Reidel SP, Camp VE, Ross ME, Wolff JA, Martin BS, Tolan TL, Wells RE (eds) The Columbia River Flood Basalt Province, Geol Soc Am Spec Pap, vol 497, pp 1–43

Ryan MP, Sammis CG (1978) Cyclic fracture mechanisms in cooling basalt. Geol Soc Am Bull 89:1295–1308

Sakuyama T, Tian W, Kimura JI, Fukao Y, Hirahara Y, Takahashi T, Senda R, Chang Q, Miyazaki T, Obayashi M, Kawabata H, Tatsumi Y (2013) Melting of dehydrated oceanic crust from the stagnant slab and of the hydrated mantle transition zone: constraints from Cenozoic alkaline basalts in eastern China. Chem Geol 359:32–48

Self S, Keszthelyi L, Thordarson T (1998) The importance of Pahoehoe. Annu Rev Earth Planet Sci 26:81–110

Sheth HC (2018) A photographic atlas of flood basalt volcanism. Springer, New York, 363 + xvi p.

Sheth HC, Ray JS, Senthil KP, Duraiswami RA, Chatterjee RN, Gurav T (2011) Recycling of flow-top breccia crusts into molten interiors of flood basalt lava flows: field and geochemical evidence from the Deccan Traps. In: Ray J, Sen G, Ghosh B (eds) . Springer, Topics in igneous petrology, pp 161–180

Sheth H, Meliksetian K, Gevorgyan H, Israyelyan A, Navasardyan G (2015) Intracanyon basalt lavas of the Debed River (northern Armenia), part of a Pliocene-Pleistocene continental flood basalt province in the south Caucasus. J Volcanol Geotherm Res 295:1–15

Sheth H, Pal I, Patel V, Samant H, D'Souza J (2017a) Breccia-cored columnar rosettes in a rubbly pāhoehoe lava flow, Elephanta Island, Deccan Traps, and a model for their origin. Geosci Front 8: 1299–1309

Sheth H, Patel V, Samant H (2017b) Control of early-formed vesicle cylinders on upper crustal prismatic jointing in compound pāhoehoe lavas of Elephanta Island, western Deccan Traps, India. Bull Volcanol 79:63. https://doi.org/10.1007/s00445-017-1147-3

Smith AD (1998) The geodynamic significance of the DUPAL anomaly in Asia. In: Flower MFJ, Chung SL, Lo CH, Lee TY (eds) Mantle dynamics and plate interactions in East Asia, Geodynamics Series, vol 27. American Geophysical Union Press, Washington, D.C., pp 89–105

Sommer E (1969) Formation of fracture 'lances' in glass. Engineering Fracture Mechanics 1:539–546

Spry AH (1962) The origin of columnar jointing, particularly in basalt flows. J Geol Soc Aust 8:191–216

Tanner LH (2013) Surface morphology of basalt columns at Svartifoss, VatnajökulsÞjóðgarður. Southern Iceland. J Geological Res:1–8

Tomkeieff SI (1940) The basalt lavas of the Giant's Causeway district of Northern Ireland. Bull Volcanol 6:89–146

Walker GPL (1972) Compound and simple lava flows and flood basalts. Bull Volcanol 35:590

Waters AC (1960) Determining direction of flow in basalts. Am J Sci 258-A:350–366

Weinberger R, Burg A (2019) Reappraising columnar joints in different rock types and settings. J Struct Geol 125:185–194

Wilmoth RA, Walker GPL (1993) P-type and S-type pahoehoe: a study of vesicle distribution patterns in Hawaiian lava flows. J Volcanol Geotherm Res 55:129–142

Woodell DR (2009) Constraints on formation of columnar joints in basaltic lava. B.A. Thesis. Colonado College 1–18

Wright TL, Okamura RT (1977) Cooling and crystallization of tholeiitic basalt, 1965 Makaopuhi lava lake, Hawaii, U.S. Geol. Surv. Prof. Pap 1004:1–78

Xu SN (1982) Discussion on the morphological and genetical classification of columnar joints in basalt. Journal of Hangzhou University 9: 447–498 (in Chinese with English abstract)

Xu SN (1984) Discovery of cyclic stria on the surface of columnar joints in Cenozoic basalts in eastern Zhejiang and its significance. Geol Rev 30:586–595 (in Chinese with English abstract)

Xu Z, Zhao ZF, Zheng YF (2012) Slab-mantle interaction for thinning of cratonic lithospheric mantle in North China: geochemical evidence from Cenozoic continental basalts in central Shandong. Lithos 145–147:202–217

Zeng G, Chen LH, Xu XS, Jiang SY, Hofmann AW (2010) Carbonated mantle sources for Cenozoic intra-plate alkaline basalts in Shandong, North China. Chem Geol 273:35–45

Zeng G, Chen LH, Yu X, Liu JQ, Erdmann S (2017) Magma-magma interaction in the mantle beneath eastern China. J Geophys Res (Solid Earth). 122:2763–2779. https://doi.org/10.1002/2017JB014023

Zhang JC, Lu QD (1997) On the characteristics and origin of the Cenozoic basalts in Fujian Province. Geology of Fujiang 1:1–9 (in Chinese with English abstract)

Zhao HL, Di YJ, Liu ZW, Li J, Deng JF, He GS, Liu QH (2004) Cenozoic volcanism and mantle plume along southeast coast of China. Acta Geol Sinica 78:781–788 (in Chinese with English abstract)

Zhi XC (1990) Trace element geochemistry of Tertiary continental alkalic basalt from Liuhe-Yizheng, Jiangsu Province, China. Acta Petro Sinica 6(2):30–42 (in Chinese with English abstract)

Zhou XM, Chen TH (1981) Composition and evolution of Cenozoic basaltic rocks in southeastern coastal provinces of China. Acta Geol Sinica 1:29–40 (in Chinese with English abstract)

Zou HB, Zindler A, Xu X, Qi Q (2000) Major, trace element, and Nd, Sr and Pb isotope studies of Cenozoic basalts in SE China: mantle sources, regional variations, and tectonic significance. Chem Geol 171:33–47